Paleoceanography and Paleoclimatology

RESEARCH ARTICLE
10.1029/2024PA004902

Key Points:

- We evaluate past and future hydroclimate patterns in the Mississippi River Basin from 850 to 2100 CE in the Community Earth System Model Last Millennium Ensemble
- The basin is wetter during the 20th century compared to the pre-industrial period, but shifts toward drier conditions in the 21st century
- Single-forcing experiments reveal a dominant role of land use/land cover changes in modulating basin hydroclimate

Supporting Information:

Supporting Information may be found in the online version of this article.

Correspondence to:

K. Murphy,
kam23@rice.edu

Citation:

Murphy, K., Dee, S., Doss-Gollin, J., Dunne, K. B. J., O'Donnell, M., & Muñoz, S. (2024). Competing influences of land use and greenhouse gas emissions on Mississippi River Basin hydroclimate simulated over the Last Millennium. *Paleoceanography and Paleoclimatology*, *39*, e2024PA004902. https://doi.org/10.1029/2024PA004902

Received 15 JUN 2023
Accepted 11 JUN 2024

Competing Influences of Land Use and Greenhouse Gas Emissions on Mississippi River Basin Hydroclimate Simulated Over the Last Millennium

Kelsey Murphy[1], Sylvia Dee[1], James Doss-Gollin[2], Kieran B. J. Dunne[3], Michelle O'Donnell[4,5], and Samuel Muñoz[4,5]

[1]Department of Earth, Environmental, and Planetary Sciences, Rice University, Houston, TX, USA, [2]Department of Civil and Environmental Engineering, Rice University, Houston, TX, USA, [3]Faculty of Civil Engineering and Geosciences, Delft University of Technology, Delft, The Netherlands, [4]Department of Marine and Environmental Sciences, Marine Science Center, Northeastern University, Nahant, MA, USA, [5]Department of Civil and Environmental Engineering, Northeastern University, Boston, MA, USA

Abstract The Mississippi River is a vital economic corridor used for generating hydroelectric power, transporting agricultural products, and municipal and industrial water use. Communities, industries, and infrastructure along the Mississippi River face an uncertain future as it grows more susceptible to climate extremes. A key challenge is determining whether Mississippi river discharge will increase or decrease during the 21st century. Because the 20th century record is limited in time, paleoclimate data and model simulations provide enhanced understanding of the basin's hydroclimate response to external forcing. Here, we investigate how anthropogenic forcing in the 20th century shifts the statistics of river discharge compared to a Last Millennium (LM) baseline using simulations from the Community Earth System Model Last Millennium Ensemble. We present evidence that the 20th century exhibits wetter conditions (i.e., increased river discharge) over the basin compared to the pre-industrial, and that land use/land cover changes have a significant control on the hydroclimatic response. Conversely, while precipitation is projected to increase in the 21st century, the basin is generally drier (i.e., decreased river discharge) compared to the 20th century. Overall, we find that changes in greenhouse gases contribute to a lower risk of extreme discharge and flooding in the basin during the 20th century, while land use changes contribute to increased risk of flooding. The additional climate information afforded by the LM simulations offers an improved understanding of what drove extreme flooding events in the past, which can help inform the development of future regional flood mitigation strategies.

1. Introduction

Between 1980 and 2022, the United States (US) experienced 37 "billion-dollar" flooding events, with a total cost of $177.9 billion dollars. During that same time, there have been 30 "billion-dollar" US drought events, costing a total of $327.7 billion dollars (Smith, 2020). Both the frequency and intensity of heavy precipitation and drought events are expected to increase in response to higher global temperatures, especially in regions already prone to these hazards (IPCC, 2022). Consequently, the total costs of these billion-dollar water-related events will likely continue to rise. Many regions over the continental US are expected to see an increase in heavy precipitation; the Southwest and Southern Great Plains are likely to remain particularly susceptible to intense drought periods (Hayhoe et al., 2018).

The Mississippi River Basin (MRB), which covers about 40% of the US, is no exception to changing hydroclimatic hazards as greenhouse warming continues. In 2011, the Mississippi River and Tributaries (MR&T) project, a system of floodways, spillways, and levees initiated in the 1928 Flood Control Act, withstood one of the largest flooding events in the observational period on the Lower Mississippi River (DeHaan et al., 2012). However, the suitability of the MR&T design for extreme hydroclimate events (e.g., flooding and low-flows) in the future remains unclear (DeHaan et al., 2012), especially as the statistics of these events are changing rapidly. Indeed, it is hypothesized that river engineering and natural climate variability may have increased the risk of recent flooding events in the MRB, and will continue to do so in the future (Munoz et al., 2018). For example, Törnqvist et al. (2020) found that levees have redirected the flow of land-replenishing sediments toward the Gulf of Mexico and away from Mississippi River Delta marshlands, causing subsidence and inundating marshlands, which provide natural protection against storm surges (Batker

et al., 2014; Leonardi et al., 2018). Low flows also have devastating impacts. The National Oceanic and Atmospheric Administration's National Centers for Environmental Information reported on the record-breaking droughts of October 2022 along the Mississippi River, revealing that such lows have not been seen in at least a decade; the 2022 low-flow event disrupted barge traffic at critical inland ports, including Memphis, TN and Vicksburg, MS (Assessing the U.S. Climate in October 2022, 2022). Despite these navigation concerns accompanying low-flow events, Amorim et al. (2023) find that *higher* water levels are more often associated with obstructed travel along the lower Mississippi River, specifically in the years 1963–2020. Broadly speaking, agriculture, manufacturing and recreation industries all rely on a functioning navigation system along the channel, and both flooding and drought can disrupt global supply chains tied to the MRB via destruction of croplands and port infrastructure or delays in the transport of goods along the channel (Levermann, 2014).

Understanding how hydroclimate extremes will evolve across the MRB in the future in response to anthropogenic and natural climatic change is of critical importance (C. Raymond et al., 2020), but we have a limited understanding of how the MRB hydroclimate will respond to rapid climate change (Seneviratne et al., 2021) as climate model projections disagree on how greenhouse gas forcing will influence river discharge. A key challenge is predicting whether future hydroclimate conditions across the Lower MRB will increase or decrease during the 21st century (Tao et al., 2014; Van der Wiel et al., 2018). Both precipitation and evaporation are predicted to increase, while hydrologic contributions due to snow melt are expected to decrease (Georgakakos, 2014; Lewis et al., 2019). A warmer atmosphere drives an increase in water vapor and extreme precipitation due to the Clausius-Clapeyron relationship (Held & Soden, 2006; Ivancic & Shaw, 2016), but alongside the increase in temperature, there will be less precipitation falling as snow. Changes in both greenhouse gas concentrations (GHG) and land use/land cover (LULC) have demonstrable impacts on the Mississippi's flood regime, but debate remains surrounding the dominance of each on runoff, and surrounding their impacts on the magnitude and frequency of extreme flooding events in the MRB (Foley et al., 2004; Frans et al., 2013; Jha et al., 2004; Lewis et al., 2023; Mishra et al., 2010; Pinter et al., 2008; Qian et al., 2007; Rossi et al., 2009; Schilling et al., 2008, 2010; Tran & O'Neill, 2013). Natural variability also influences trends in precipitation (Eischeid et al., 2023) and runoff (Hoell et al., 2023) in ways that are different from what might be expected from LULC changes alone. Recent work from Marvel et al. (2021) show how high emissions scenarios (i.e., increased GHG forcing) might lead to seasonal changes in peak evaporation, runoff, and soil moisture in parts of the US. Broadly speaking, however, land-atmosphere feedbacks are not completely understood, and climate models do not perfectly capture how anthropogenic activities, such as deforestation or afforestation, impact the hydrologic cycle (Bonan, 2008; L. Chen & Dirmeyer, 2020).

Resolving the various long-term controls on MRB hydroclimate requires data spanning long timescales to accurately filter the effects of quasi-periodic modes of variability. However, instrumental records for MRB discharge are relatively short: five United States Geological Survey (USGS) streamgage locations across the Lower Mississippi and its major tributaries are plotted in Figure 1. These annual river discharge data sets extend back only to the early 20th century. Paleoclimate model simulations spanning the Last Millennium (LM) extend 20th century observations hundreds of years into the past, increase the number of hydroclimate events in our sample size, and provide a baseline against which we can compare anthropogenic changes to natural climate variability in the Pre-Industrial (PI) era (Hansen & Sato, 2012; Munoz et al., 2018).

To bolster estimates of and contextualize future MRB hydroclimate risks, here we use a fully coupled global climate model spanning 850–2100 CE, the Community Earth System Model version 1.2 Last Millennium Ensemble (CESM-LME). CESM includes a river transport model (RTM) to simulate monthly discharge data (Branstetter, 2001; Branstetter & Famiglietti, 1999), making it particularly well-suited to this work. The CESM-LME also includes single-forcing simulations that enable detection/attribution of hydroclimate change to both anthropogenic and natural forcings, partitioning the individual impacts of GHG or LULC forcing, for example (Schurer et al., 2013). Finally, the CESM-LME contains 13 full-forcing simulations, with 4 members that extend into the 21st century (Kay et al., 2015; Otto-Bliesner et al., 2016). These simulations spanning the LM afford a baseline range for natural variability against which we compare anthropogenic changes in hydroclimate and MRB discharge simulated in the 20th–21st centuries. While a number of previous studies have evaluated global and U. S. hydroclimate in the CESM-LME in response to both full (Atwood et al., 2021; Bhattacharya & Coats, 2020; Fasullo et al., 2019; Munoz & Dee, 2017; Otto-Bliesner et al., 2016; Steiger et al., 2018; Tejedor et al., 2021a, 2021b; Wiman et al., 2021) and single-forcing (Stevenson et al., 2016, 2018) experiments, to-date, no studies

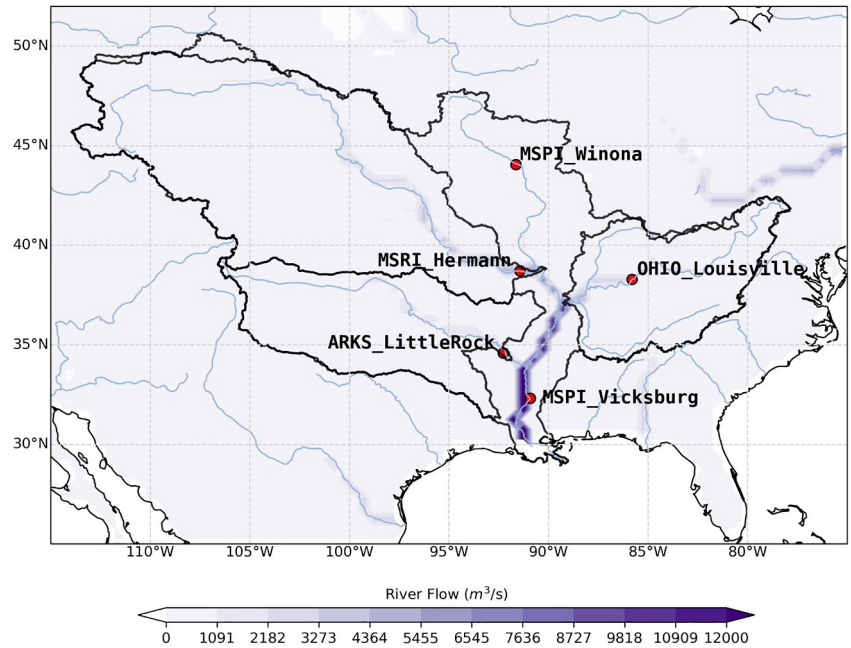

Figure 1. Map of annual discharge (m^3/s) averaged over the 20th century in the Mississippi River Basin (MRB). Key United States Geological Survey sites include Winona, MN in the Upper MRB, Louisville, OH in the Ohio River basin, Hermann, MO in the Missouri River basin, Little Rock, AR in the Arkansas-White River basin, and Vicksburg, MS in the Lower MRB.

have focused on the MRB's hydroclimate and discharge response to *both* full- and single-forcing simulations from 850 to 2100 CE.

In this paper, we harness the many advantages of the CESM-LME (a river routing model, a multi-member ensemble spanning 850–2100 CE, and single-forcing experiments) to answer critical questions about the large-scale hydroclimate responses of the MRB system to different external forcing conditions. We attempt to diagnose the controls on MRB discharge and isolate how hydroclimate patterns amplify or dampen river flows. We focus our analyses on three key questions:

1. How does MRB discharge respond to greenhouse gas forcing in the 20th century compared to the PI?
2. What are the key hydroclimatic processes that drive changes in MRB discharge and where in the basin do they occur? Which external forcings have the greatest impacts on these drivers?
3. How are the statistics of MRB discharge projected to change through the 21st century given the changes in land use and elevated greenhouse gas forcing?

As mentioned above, we have highly incomplete constraints on the future magnitude of MRB discharge; 20th century observations alone cannot completely represent the statistical distribution of potential hazards that will transpire. In order to avoid the losses caused by extreme climate change events, we must first better understand the climate drivers of future risk.

2. Data and Methods

A mechanism-based approach is taken to identify drivers of future MRB hydroclimate. We look at the MRB's response to both anthropogenic and natural forcing experiments across the key LM periods in the PI and the 20th and 21st centuries, as well as the relative changes in magnitude and frequency of extreme flooding under different external forcing scenarios.

2.1. LM Ensemble Forcing Simulations

We use an ensemble of climate model simulations from the CESM-LME in an effort to compare PI to historical and future (20th and 21st century) projections of Lower MRB hydroclimate (Hurrell et al., 2013; Kay et al., 2015; Otto-Bliesner et al., 2016). The model has a horizontal resolution of the atmospheric and land components of ~2°,

and ocean components of ∼1°. While relatively coarse, this grid scale facilitates a large ensemble size and long integration over the LM while balancing the need for computational efficiency (Otto-Bliesner et al., 2016). Specifically, we evaluate changes in the model output variables precipitation (calculated as the sum of convective and large-scale precipitation, PRECC + PRECL), soil moisture (SOILLIQ), runoff (QRUNOFF), snow melt (QSNOMELT), evapotranspiration (calculated as the sum of ground and canopy evaporation plus transpiration, QSOIL + QVEGE + QVEGT), and river discharge (QCHANR) for the period 850–2100 CE. Soil moisture in kg/m^2 is averaged over the depth column for each grid cell to retrieve total soil moisture. All variables are reported as annual averages, unless noted otherwise.

The CESM-LME contains both single-forcing simulations, where the model is run with one external forcing at a time, and full-forcing simulations, which employ all external forcings (Otto-Bliesner et al., 2016). We evaluate both anthropogenic and natural forcing experiments, including greenhouse gas (GHG, $n = 3$ ensemble members), land use/land cover (LULC, $n = 3$ ensemble members), and volcanic (VOLC, $n = 5$ ensemble members). Analyses using additional anthropogenic and natural forcing experiments, including ozone-aerosol (AER, $n = 5$ ensemble members) and solar (SOLAR, $n = 4$ ensemble members) can be found in Supporting Information. All single and full-forcing ensemble members span the period 850–2005 CE, except AER-forcing simulations which only span 1850 to 2005 CE. Initial conditions are different for every ensemble member to account for internal variability (Kay et al., 2015). Thirteen full-forcing ensemble members are analyzed, four of which (members 002, 003, 008, & 009) were extended into the 21st century from 2006 to 2100 CE. We additionally employ the CESM-LME control simulation, where the model is run without any external forcing, for comparison with ensemble averages derived from the full and single-forcing experiments. This allows us to identify hydroclimate signals driven by each individual forcing against a background with internal climate variability alone.

We provide "single-forcing minus control run" analyses to highlight the impacts of anthropogenic climate change (e.g., GHG), and also explore the influence of natural forcings such as volcanic eruptions on MRB hydroclimate. We use the VOLC forcing data employed in the CESM-LME simulations to extract eruption years, defined in this study as years with reconstructed radiative forcing (Gao et al., 2008) less than or equal to −0.2 W/m^2. We compare eruption years to non-eruption years (defined as years with zero radiative forcing) for each individual ensemble member. Using the threshold of −0.2 W/m^2 allows us to detect not only the hydroclimatic response during the eruption year, but the persistence of volcanic forcing in the years following an eruption. Additional documentation detailing how volcanic forcing is applied in the CESM-LME is available in Otto-Bliesner et al. (2016) and Stevenson et al. (2016). Non-eruption year composite averages were computed and subtracted from eruption years to calculate the differences for precipitation, runoff, snow melt, soil moisture, and evapotranspiration. To determine regional impacts of individual natural and anthropogenic climate forcings, we compare key periods, including the Medieval Climate Anomaly (MCA, 950–1250 CE), Little Ice Age (LIA, 1400–1800 CE), 20th century (1901–2000 CE), and 21st century (2001–2100 CE) as defined in S. Dee et al. (2020); Grove (1988); Jones and Mann (2004); Lamb (1965, 1977); Mann et al. (2009); Otto-Bliesner et al. (2016). To analyze river discharge in each basin, we find the grid cells with maximum modeled river discharge nearest to the USGS stations in Figure 1. Simulated river discharge data is extracted from one grid cell in each the Lower Mississippi (32.25°N, 91.25°W), Upper Mississippi (43.75°N, 91.25°W), Ohio River (38.25°N, 86.25°W), Arkansas-White River (34.75°N, 92.25°W), and Missouri River (38.75°N, 91.25°W). Probability density functions (PDF) are estimated using the kernel density estimation function available in the Python Seaborn library (Waskom et al., 2017). We employ a two-tailed *t*-test with a 95% confidence level to compare the difference of means at each model grid point and report statistically significant changes for the above-mentioned time periods.

2.2. CESM1.2 River Discharge Module: Validation and Comparison to Paleoclimate Reconstructions

2.2.1. Validation With USGS Stream Gage Data

Our work capitalizes on CESM1's river transport module (RTM), which routes runoff as a function of surface elevation changes through the land surface model (CLM) toward coastlines (Branstetter, 2001; Branstetter & Famiglietti, 1999) at 0.5° resolution (Oleson, 2010). The river discharge from CESM has been compared to gage station data in previous work (Dai & Trenberth, 2002), including for the lower Mississippi River (Munoz & Dee, 2017). Figure 1 confirms that the CESM1 RTM accurately routes discharge (geographically) in the Mississippi corridor overlapping with USGS river gage stations. Streamflow data from the USGS stations in Figure 1

have formed the basis for validation of the RTM in previous work. To document the performance of the CESM1 RTM, Dunne et al. (2022) provide a comparison between modeled and observed discharge at Vicksburg, Mississippi (Dunne et al., 2022, Figure 1). CESM1 RTM generally captures the statistics of flow in both the mean and ensemble spread, supporting its use for this analysis. As shown in Munoz and Dee (2017), CESM1 contains biases in the seasonality and timing of peak flows on the lower Mississippi; simulated river discharge is at its maximum in June, while observed flows peak in spring (May or earlier). The model generally captures the key processes that cause peaks in discharge (Munoz & Dee, 2017, Supplemental Figure 1). Snow melt and precipitation, hydrologic mechanisms that are significant drivers of flooding in the region, also show seasonal biases, but the sequence of hydrologic events ultimately follow that seen in observations (see O'Donnell et al., 2022 and Figure S1 in Supporting Information S1 which shows monthly data from CESM1 compared to European Center for Medium-Range Weather Forecasts (ECMWF) Reanalysis v5 (ERA5) snow melt and runoff data (Hersbach et al., 2020, 2023), Global Precipitation Climatology Centre (GPCC) precipitation data (Becker et al., 2013; Schneider et al., 2017), and observed river discharge data from USGS).

CESM1 overestimates precipitation and runoff in the western US (Danabasoglu et al., 2020; Lehner et al., 2019). Hoell et al. (2024) demonstrates the same positive bias for the Upper Missouri River basin, but reports similar seasonal cycles in CESM1 compared to observational data. We find that the magnitude and sign of changes from the PI to the 20th century are similar across all months for most of the hydroclimate variables and basins - suggesting consistent shifts in the annual average (Figure S9 in Supporting Information S1). However, there are noticeable differences in the sign of precipitation and the magnitude of the runoff response for the 20th century compared to the PI. Colder (warmer) months are associated with higher (lower) rates of precipitation in the 20th century in the Lower and Upper Mississippi and Ohio River basins. Increases in March–June runoff are larger during the 20th century compared to those in other months over the Upper Mississippi basin (Figure S9 in Supporting Information S1). Based on this and the previous work exploring the impacts of seasonal hydroclimate variability in the MRB (Dunne et al., 2022; Munoz & Dee, 2017), we expect these seasonal biases are unlikely to affect our analysis of decadally-averaged mean state projections for relative changes in discharge over the LM through the 21st century.

Finally, the CESM1 RTM model simulations do not include any anthropogenic groundwater extraction and water use, tile drainage, artificial barriers, or reservoir regulation effects; however, the goal of our work is to compare relative changes in large-scale climate and discharge statistics between past and future time periods spanning multiple decades. Moreover, validating the model against observations is complicated by the strong human management of the MRB through mechanisms such as reservoirs. While flood control structures have important and demonstrable impacts on river discharge (Munoz et al., 2018), we instead focus on large-scale climate changes and shifts likely to induce changes in the statistics of discharge over decadal timescales.

2.2.2. Comparison With Available Paleoclimate Reconstructions

We further compared discharge and hydroclimate in CESM1 to available paleoclimate reconstructions spanning the LM. We briefly summarize CESM1's performance in comparison to these reconstructions here:

- *NADA*: First, we compare simulated June–August (JJA) soil moisture to the reconstructed JJA Palmer Drought Severity Index (PDSI) from the North American Drought Atlas (Cook et al., 2004, 2010, NADA). Figure S2 in Supporting Information S1 compares the spatial difference between the 20th century and PI, defined here as 1385–1850 CE (due to temporal constraints of NADA), for both the CESM-LME soil moisture and NADA PDSI. Figure S3 in Supporting Information S1 compares the time series of simulated soil moisture and reconstructed PDSI from 1385 to 2000 CE over the Lower MRB. Broadly, the comparison suggests that CESM1 simulates lower soil moisture conditions compared to reconstructed PDSI from tree rings (i.e., the model has a bias toward drier conditions than reconstructions for 20th century minus PI).
- *NASPA*: CESM-simulated cool (December-April) and warm (May–July) season precipitation is also compared to reconstructed precipitation from the North American Seasonal Precipitation Atlas (Stahle et al., 2020, NASPA) from 850 to 2000 CE. Figure S4 in Supporting Information S1 compares the difference of 20th century minus PI for both CESM-LME and NASPA cool and warm season precipitation, and suggests modeled precipitation is lower compared to reconstructed precipitation from tree rings. Figures S5 and S6 in Supporting Information S1 offer further comparison of the distributions for

total precipitation in CESM-LME and NASPA from 850 to 2005 CE. Over the LM, the model has a bias toward drier conditions compared to reconstructions during the cool season, with the exception of the Missouri River basin (Figure S5 in Supporting Information S1). However, the model appears to overestimate warm season precipitation, especially evident in the Ohio River, Arkansas-White River, and Missouri River basins (Figure S6 in Supporting Information S1).

Streamflow Reconstructions: Simulated JJA river discharge is compared to reconstructed JJA streamflow from the Arkansas-White River (Cleaveland, 2000) from 1023 to 1985 CE. Additionally, simulated river discharge for water years (October-September) 851–2005 CE is compared to reconstructed streamflow in the Upper Missouri River (Martin et al., 2019, 2020). We define the Upper Missouri River region using the location of 29 naturalized streamflow records (Figure S8 in Supporting Information S1) employed in Martin et al. (2019). The CESM-LME has a bias toward higher river discharge when compared to both streamflow reconstructions, shown in Figure S7 in Supporting Information S1. Finally, LM trends in reconstructed Lower Mississippi river discharge (Wiman et al., 2021) and lower Ohio River floods (Gibson et al., 2022) are consistent with those in the CESM-LME full-forcing simulations; river discharge is lowest in the MCA and increases toward present (Wiman et al., 2021, Figure 4).

Validation against the above-mentioned paleoclimate reconstructions broadly suggests that CESM1 is biased toward lower soil moisture and precipitation, but higher river discharge. Note, however, that NADA and NASPA are on different grids (2.5° and 0.5°, respectively) compared to the land and atmosphere components of the CESM-LME. These comparisons highlight important biases within the model (see Discussion), and provide context for our analyses of drivers of large-scale hydroclimate patterns over the LM.

2.3. Land Use Change

We use the Land Use Harmonization[2] historical data set (LUH2 v2h) to diagnose how LULC changes from the 11th to 20th century influenced simulated runoff over the LM (G. Hurtt et al., 2019; G. C. Hurtt et al., 2020). The LUH2 v2h data set includes 12 different "states of land use" variables: forested primary and potentially forested secondary land, non-forested primary and potentially non-forested secondary land, managed pasture, range land, urban land, C3 annual, perennial, and nitrogen-fixing crops, and C4 annual and perennial crops (G. Hurtt et al., 2019; G. C. Hurtt et al., 2020). The units for each state variable are "fraction of grid cell" and a time series for all LUH2 v2h land use types can be found in Figure S12 in Supporting Information S1. In our analysis, we group forested primary and potentially forested secondary land as "forest," non-forested primary and potentially non-forested secondary land as "non-forested," managed pasture and range land as "pasture," and all C3 and C4 crops as "crops," assuming similar Manning's N values for each land use type (Arcement & Schneider, 1989; Engman, 1986). The CESM1 RTM, however, uses a simplified equation dependent on mean topographic slope to calculate flow velocity rather than the Manning's N equation (For further detail on flow velocity calculations, please refer to Oleson et al. (2013)). The transient land forcing files have a constant mean land elevation for all years in the CESM-LME simulations (Figure S13 in Supporting Information S1). Note that prior to the 19th century, over most of the basin, changes in land use are minor.

2.4. Risk Ratios and Annual Exceedance Probabilities

Risk ratios are commonly employed to attribute climate change to anthropogenic forcing, though this approach has not yet been applied to discharge projections for the MRB (Kirchmeier-Young et al., 2017; Swain et al., 2020; Touma et al., 2021). We compute risk ratios to evaluate how different external forcings change the likelihood of increased or decreased discharge in the Lower MRB. To compute risk ratios, we first pool all of the full-forcing ensemble members together into one distribution to calculate the 95th percentile of monthly average discharge at Vicksburg, Mississippi (data is extracted from the grid cell centered at 32.25°N, 91.25°W; Dunne et al., 2022). We then pool all ensemble members from each single-forcing simulation into individual distributions, and determine the frequency with which the monthly discharge values in each single-forcing distribution exceeds the full-forcing 95th percentile threshold (results are qualitatively similar for other thresholds, not shown). Here, we assume (a) stationarity and (b) each year from each ensemble member is independent and identically distributed. By using distributions with all ensemble members pooled together, we are able to integrate over the randomness (i.e., internal variability) of the individual ensemble members. The frequencies calculated in the step above are divided by the number of elements (monthly discharge values) along the time axis to obtain the probability of exceedance for each single-forcing simulation. Finally, the risk ratios are computed by dividing the probability of

a discharge event exceeding the 95th percentile in each single-forcing simulation by the probability of an event exceeding the same threshold in all full-forcing members:

$$RR = P_{single-forcing}/P_{full} \quad (1)$$

where RR is the risk ratio, $P_{single-forcing}$ is the frequency with which single-forcing exceeds the threshold, and P_{full} is the frequency with which full forcing exceeds the threshold. A risk ratio greater than one indicates an increased risk of high discharge and a risk ratio less than one indicates a decreased risk of high discharge.

To calculate annual exceedance probabilities, we first find the annual maxima for all CESM-LME discharge data (850–2005 CE) at Vicksburg, Mississippi. For each individual forcing ensemble (Full, GHG, LULC, VOLC), we pool the discharge maxima and then rank them to develop four different empirical distributions. We then find the annual maximum discharge values associated with annual exceedance probabilities ranging from 0.5% to 50% for each of the individual forcing series. Finally, the annual exceedance probabilities are used to compare differences in discharge amongst the various single-forcing ensembles. By utilizing the annual maxima from all members of each forcing series, we are able to expand the available number of years of data (assuming stationarity) and perform a more robust flood frequency analysis. For example, there are 13 full forcing ensemble members each with 1156 years (850–2005 CE) of data. Thus, if we combine all full forcing members into a larger distribution, there are a total of 15,028 annual maxima (Table 2 lists the total number of annual maxima for all forcing ensembles).

Risk ratios and annual exceedance probabilities for AER-only and SOLAR-only are included in Table S2 and Figure S15 in Supporting Information S1. The AER forcing simulations only span 1850 to 2005 CE, so AER is not included in the PI risk ratio calculations (Table S2 in Supporting Information S1). It is important to note that the discharge data used to calculate risk ratios and annual exceedance probabilities has not been bias corrected, and the analyses provided in this section are solely used as a useful technique to quantify relative changes across the different external forcing ensembles.

3. Results: Simulated Discharge and Hydroclimate in the MRB From 850 to 2100 CE

Changes in LULC prove to be an important control on modeled runoff and discharge compared to GHG and VOLC forcing (Section 3.1). Simulated past and future hydroclimate patterns in the MRB show the basin is generally wetter during the 20th century compared to the PI, but shifts again toward drier conditions in the 21st century (Section 3.2). Here, wetter (drier) conditions refers to an increase (decrease) in discharge, precipitation, soil moisture, runoff, and/or snow melt and a decrease (increase) in evapotranspiration. Risk ratios and annual exceedance probabilities suggest discharge decreases under GHG forcing and increases under LULC forcing in the 20th century (Sections 3.3 and 3.4).

3.1. Control Run and Single-Forcing Experiments

We first compare shifts in river discharge for each basin in response to full forcing (Figure 2), GHG forcing (Figure 3), and LULC forcing (Figure 4) during the 20th century, MCA, and LIA. Table 1 summarizes these changes and emphasizes that, in the 20th century compard to the LM, LULC forcing drives statistically significant shifts toward higher river discharge compared to GHG forcing. In the full forcing ensemble, river discharge is lowest during the MCA and increases toward present in the Lower and Upper Mississippi River and Ohio River (Figure 2). These patterns are consistent with previous work suggesting that regions in North America may have been warmer and drier during the MCA before transitioning into colder, wetter conditions during the LIA (S. Dee et al., 2020; Herweijer et al., 2006, 2007; Mann et al., 2009; Rustic et al., 2015; Stevenson et al., 2018; Trouet et al., 2009). The 20th century exhibits significantly higher river discharge in the Lower and Upper Mississippi River and Ohio River, and significantly lower river discharge in the Arkansas-White River basin in the full forcing experiments (Table 1). Table S1 and Figure S11 in Supporting Information S1 extend this analysis, comparing late 19th and late 20th century river discharge under AER-only simulations. AER forcing drives statistically significant shifts toward higher river discharge in the Upper Mississippi River and Missouri River basins in the 20th century (Figure S11 in Supporting Information S1).

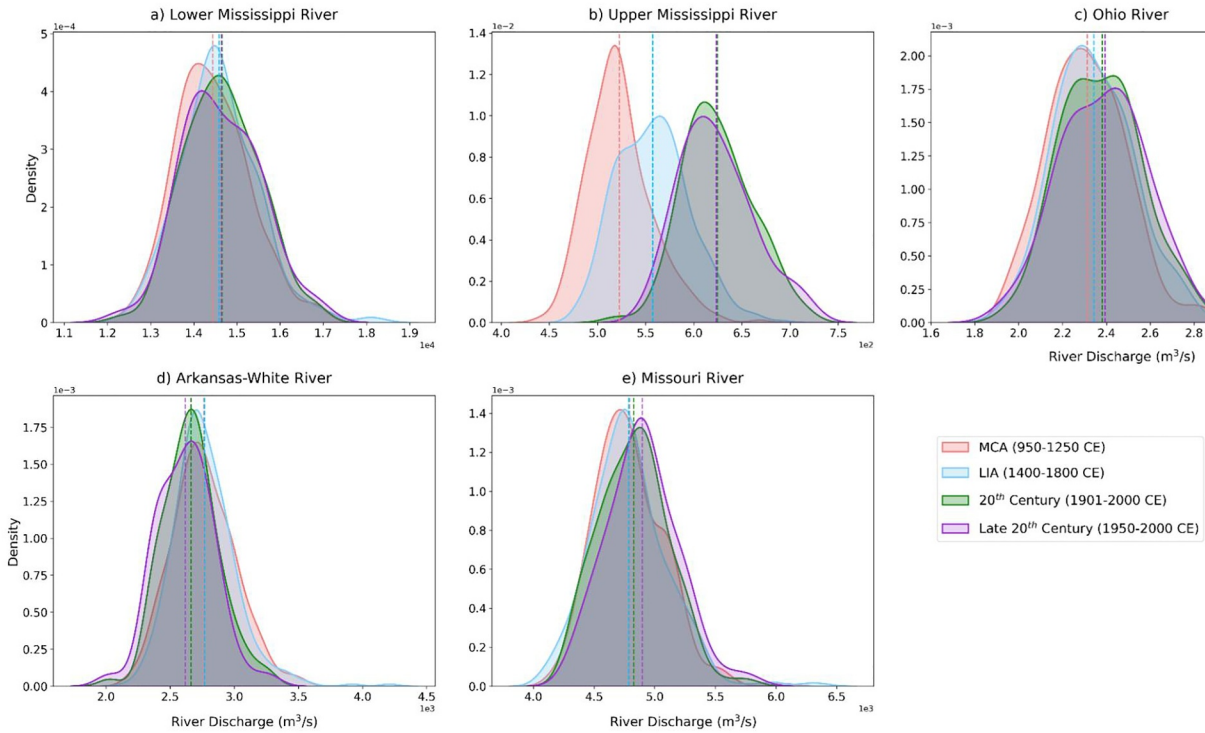

Figure 2. PDFs for annual discharge (m^3/s) from one grid cell in the (a) Lower Mississippi (32.25°N, 91.25°W), (b) Upper Mississippi (43.75°N, 91.25°W), (c) Ohio River (38.25°N, 86.25°W), (d) Arkansas-White River (34.75°N, 92.25°W), and (e) Missouri River (38.75°N, 91.25°W) basin under full-forcing during the MCA, LIA, and 20th century. Distributions consist of data from all 13 full-forcing members. Dashed vertical lines indicate distribution means.

The PDFs (and time series provided in Figure S10 in Supporting Information S1) afford little information about the spatial heterogeneity of these hydroclimate shifts over the LM. Therefore, we next evaluated hydroclimate pattern changes as mapped differences between the control run and single-forcing (GHG, LULC) experiments during the MCA, LIA, and the 20th century (Figures 5–9). Both GHG and LULC forcing lead to overall drier conditions during the LIA and wetter conditions for the MCA compared to the control (Figures 5–9a,b,d,e). The most notable changes in MRB hydroclimate appear in the 20th century, implying that GHG and LULC forcing have a strong influence on runoff, precipitation, soil moisture, snow melt, and evapotranspiration after the start of the Industrial Revolution. However, Figures 7 and 8 also show significant changes in soil moisture and runoff during the MCA and LIA compared to the control run. Statistical significance is most consistent across the MRB in the "LULC forcing minus control run" experiments during the 20th century (Figures 5–9f). Spatially significant changes in evapotranspiration occur under both GHG and LULC, although the sign of the response varies (Figures 9c and 9f). While there is spatial heterogeneity across the basin, the GHG and LULC single-forcing experiments generally lead to increased precipitation during the 20th century compared to the control run (Figures 5c and 5f). GHG and LULC exert opposite forcings on 20th century snow melt, with GHG (LULC) driving drier (wetter) conditions (Figures 6c and 6f). Additionally, the LULC forcing ensemble exhibits wetter conditions in the Missouri River basin, Arkansas-White basin, and Upper MRB; this is due to increases in simulated soil moisture and runoff during the 20th century compared to the GHG forcing ensemble (see Figures 7–8c,f).

To diagnose how CESM's LULC forcing affects the spatial hydroclimate changes observed in the "single-forcing minus control" evaluation presented in Figures 5–9, we assessed changes in land use employed in the LUH2 v2h data set (Figure 10). Figure 10 shows the progression of land use changes over the LM. In earlier centuries (11–19th), the Ohio River basin, Lower and Upper MRB had a much higher percentage of forested area, while the Missouri and Arkansas-White River basins were mostly non-forested and largely without crops or pasture (Figures 10a–10f and Figure S12 in Supporting Information S1). In the 20th century, the entire eastern side of the MRB shows widespread deforestation, the majority of the Upper MRB and small sections of the Missouri and Ohio River basins show transitions to a higher percentage of cropland, and pasture becomes the dominant land

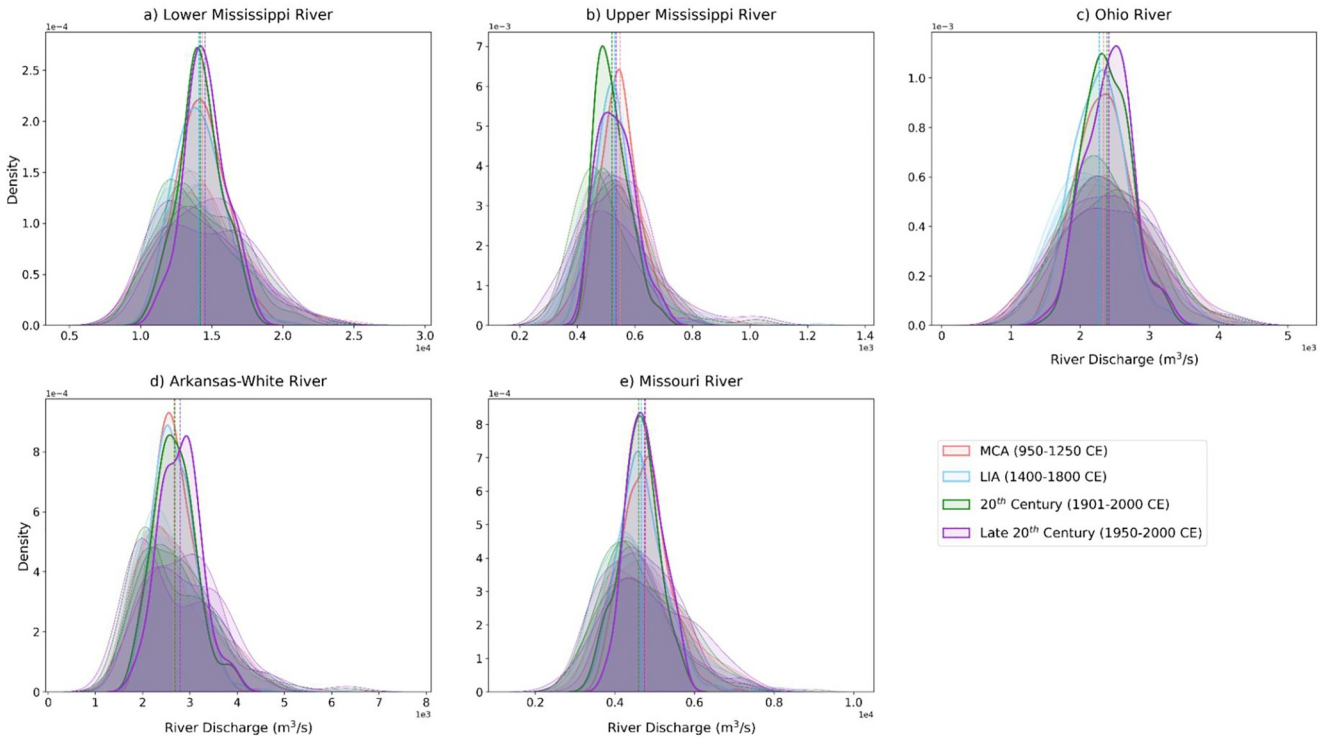

Figure 3. PDFs for annual discharge (m^3/s) from one grid cell in the (a) Lower Mississippi (32.25°N, 91.25°W), (b) Upper Mississippi (43.75°N, 91.25°W), (c) Ohio River (38.25°N, 86.25°W), (d) Arkansas-White River (34.75°N, 92.25°W), and (e) Missouri River (38.75°N, 91.25°W) basin under **GHG-only** forcing during the MCA, LIA, and 20th century. Light-colored lines represent individual ensemble members, while dark-colored lines indicate the ensemble averages. Dashed vertical lines indicate distribution means.

type in the Missouri and Arkansas-White River basins (Figures 10g–10i). These shifts in land use directly alter hydroclimate between the control and LULC-forcing ensemble via changes in runoff. Land covered by crops and pasture has largely increased since the beginning of the 18th century (Pongratz et al., 2008). Earlier studies suggest deforestation increased runoff in eastern regions of the MRB, while increased crop cover decreased runoff in western tributaries (Knox, 2001; P. A. Raymond et al., 2008; Schilling et al., 2010; Twine et al., 2004; Zhang & Schilling, 2006). A reduction in forest and vegetation cover can lead to a decrease in evapotranspiration and an increase in runoff through changes in albedo, infiltration rates, and moisture retention (Ding et al., 2022; Peña-Arancibia et al., 2019; Twine et al., 2004).

Finally, we explored the influence of VOLC forcing over the LM in the MRB. In the VOLC forcing simulations, eruption years are wetter than non-eruption years across the MRB (Figure 11). This is consistent with previous work suggesting tropical and northern-hemisphere volcanic eruptions decrease surface temperature, decrease the risk of drought, and increase soil wetness in parts of the United States (D'Arrigo et al., 2013; Stevenson et al., 2016, 2018; Tejedor et al., 2021b). There is a statistically significant decrease in evapotranspiration across the MRB (Figure 11c). A large body of literature documents the impacts of volcanic forcing on global and U.S. hydroclimate (S. Dee et al., 2020; S. G. Dee & Steiger, 2022; Stevenson et al., 2017; Tejedor et al., 2021a); we find a muted hydroclimate response driven by volcanic forcing alone compared to other single-forcing experiments over the MRB.

3.2. Pre-Industrial (PI), 20th, and 21st Century Hydroclimate Changes

We next evaluate the spatial hydroclimate response to natural and anthropogenic forcing as a function of the percent changes for the 20th century compared to PI, 21st century compared to PI, and 21st century compared to 20th century. The single-forcing ensemble members (GHG, LULC, VOLC) and full-forcing ensemble members are all evaluated independently. Overall, the full-forcing ensemble average shows that the MRB is wetter in the 20th century compared to the PI (Figures 12a–12e). The single-forcing ensembles facilitate identification of how

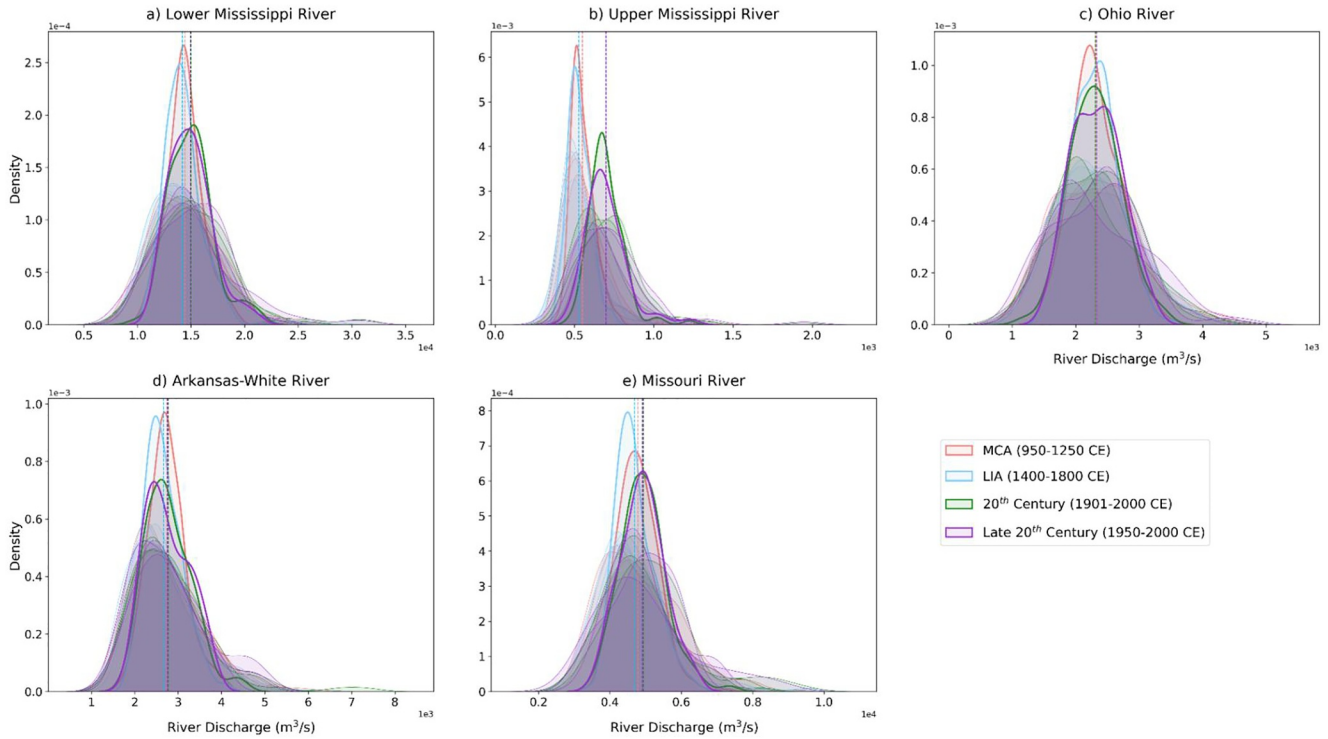

Figure 4. PDFs for annual discharge (m^3/s) from one grid cell in the (a) Lower Mississippi (32.25°N, 91.25°W), (b) Upper Mississippi (43.75°N, 91.25°W), (c) Ohio River (38.25°N, 86.25°W), (d) Arkansas-White River (34.75°N, 92.25°W), and (e) Missouri River (38.75°N, 91.25°W) basin under LULC-only forcing during the MCA, LIA, and 20th century. Light-colored lines represent individual ensemble members, while dark-colored lines indicate the ensemble averages. Dashed vertical lines indicate distribution means.

various spatial patterns of hydroclimate change modeled in the full-forcing simulations are either absent from or appear in (and are thus driven by) individual forcing changes. The columns of Figure 12 show changes in precipitation, soil moisture, evapotranspiration, snow melt, and runoff for each of the single- and full-forcing ensemble averages. The percent change in all hydroclimate variables from the PI to the 20th century due to VOLC forcing are minor compared to the LULC and GHG forcings, and thus likely contribute less to the changes seen in the full-forcing simulations. The largest averaged changes in the VOLC-only simulations occur over the Lower MRB and Arkansas-White River basin, with a 7% and 5% increase in snow melt, respectively (Figure 12s).

GHG and LULC forcing both drive statistically significant increases in precipitation in the 20th century compared to PI, but have different effects on other hydroclimate variables (Figures 12f and 12k). Under GHG forcing, evapotranspiration increases and snow melt decreases over the entire MRB (Figures 12h and 12i); GHG forcing leads to drier conditions in the MRB in the 20th century. Over the Ohio River basin and the Lower MRB, there is a significant decrease in snow melt (13% and 16%, respectively; Figure 12i) under GHG forcing. Runoff significantly decreases near the western boundary of the Upper MRB and eastern half of the Missouri River basin in the GHG simulations (Figure 12j). By contrast, under LULC forcing, soil moisture, snow melt, and runoff all significantly increase (Figures 12l,n,o), implying that LULC changes resulted in wetter conditions across the MRB in the 20th century. Soil moisture increases by 1% over the Missouri River basin and 2% over the Upper MRB under LULC forcing (Figure 12l). Snow melt increases by 14% over the Arkansas-White River basin, 17% over the Ohio River basin, and 20% over the Lower MRB (Figure 12n). Runoff increases by approximately 10% in the Missouri River basin and 13% in the Upper MRB (Figure 12o). Lastly, there is a small increase in evapotranspiration across the Lower MRB, Arkansas-White River, and Ohio River basins (Figure 12m) in the 20th century under LULC forcing. Overall, the spatial patterns under LULC forcing (Figures 12k–12o) are most similar to those in the full-forcing simulations (Figures 12a–12e) with the exception of precipitation, where both GHG and LULC forcing contribute to wetter conditions of the 20th century (Figures 12a,f,k). The largest regional changes in the full-forcing simulations occur over the Ohio River basin and Lower MRB, where snow melt increases by more than 9% from the PI to the 20th century (Figure 12d). Over the Upper MRB, runoff increases by

Table 1
Significance Testing for Full-Forcing and Single-Forcing (GHG, LULC) Distributions

20th century compared to MCA and LIA			
		20th versus MCA	20th versus LIA
Full	Lower Mississippi	**W**	W
	Upper Mississippi	**W**	**W**
	Ohio	**W**	W
	Arkansas-White	**D**	**D**
	Missouri	W	W
GHG	Lower Mississippi	D	W
	Upper Mississippi	**D**	D
	Ohio	W	**W**
	Arkansas-White	W	W
	Missouri	**D**	D
LULC	Lower Mississippi	**W**	**W**
	Upper Mississippi	**W**	**W**
	Ohio	D	W
	Arkansas-White	W	**W**
	Missouri	**W**	**W**

Note. Each column represents a comparison between two different time periods (e.g., 20th century compared to MCA). Brown "D" indicates there is lower discharge in the 20th century and blue "W" represents higher river discharge in the 20th century. Bold, underlined letters indicate a statistically significant change at the 95% confidence level.

about 5% under full forcing (Figure 12e); most of the basin exhibits statistically significant shifts toward wetter conditions (i.e., increased precipitation, soil moisture, snow melt, and runoff) in the 20th century compared to the PI (Figures 12a–12e).

Figure 12 implies that a large part of the hydroclimatic shift observed from the PI to the 20th century is driven by land use change over time. This finding is consistent with the results presented in Section 3.1 (e.g., Figure 8), showing that the LULC single-forcing simulations exhibit large shifts compared to the unforced CESM LME control run. In the Lower MRB, Upper MRB, and Ohio River basin, "forested primary land" decreases significantly at the start of the 19th century. However, "potentially forested secondary land" begins to increase after the mid-19th century and is the dominant land use type in the Lower MRB and Ohio River basin at the end of the 20th century (Figure S12a–c in Supporting Information S1). While deforestation and human-engineered drainage systems may increase runoff (Quinn & Sellinger, 1990; Twine et al., 2004), reforestation in the Ohio River basin and Lower MRB in the 20th century provides one explanation for the decreases in runoff (Figure 8f). In the Upper MRB, the conversion from "forested primary land" to mostly "C4 annual crops" and "C3 nitrogen-fixing crops" (Figure S12b in Supporting Information S1), along with a decrease in evapotranspiration (Figures 9f and 12m) and increase in snow melt (Figures 6f and 12n), may provide a partial explanation for the increases in runoff under LULC forcing (Figure 12o). Thus, we conclude that in the CESM-LME, LULC is the main driver of hydroclimate change in the MRB during the 20th century compared to the PI.

A comparison of the hydroclimate response in the late 19th and late 20th centuries under AER forcing is included in Figure S14 in Supporting Information S1. Under AER forcing, the Missouri River basin exhibits a statistically significant increase in soil moisture (1%) and runoff (4%) over a large part of the basin, while the Arkansas-White River shows a significant decrease (1%) in evapotranspiration. AER-only forcing is thus likely an additional driver of increasing soil moisture and runoff seen in the full-forcing ensemble over the Missouri River basin in the 20th century (Figures 12b and 12e).

As described in Section 2.1, only four full-forcing experiments were extended to simulate the 21st century (no single-forcing ensemble members are available past the 20th century). Figure 13 provides time series of annual discharge for all basins (1901–2100 CE) for these four full-forcing extension simulations. The Upper and Lower MRB, Arkansas-White River, and Missouri River basin projections show a decrease in discharge during the late 21st century, while the Ohio River basin shows an increase in discharge (Figure 13). PDFs and box plots of discharge in all basins during the MCA, LIA, 20th century, and late 21st century (Figures 14 and 15) indicate that all five basins have similar distributions of discharge during the MCA, LIA, and 20th century. However, there is a shift toward drier conditions for all basins except for the Ohio River Basin in the late 21st century. Full-forcing drives shifts toward significantly higher river discharge over the Ohio River basin and significantly lower discharge over the remaining basins in the 21st century compared to the 20th century (Table 3).

Table 2
Each of the Single- and Full-Forcing Ensembles (Full, GHG, LULC, VOLC) Have One Empirical Distribution, Consisting of Annual Maxima From All Ensemble Members

Forcing type	# Of ensemble members	# Of annual maxima	Description
Full	13	15,028	All available anthropogenic and natural forcings
GHG	3	3,468	Greenhouse gas forcing only
LULC	3	3,468	Land use/land cover forcing only
VOLC	5	5,780	Volcanic forcing only

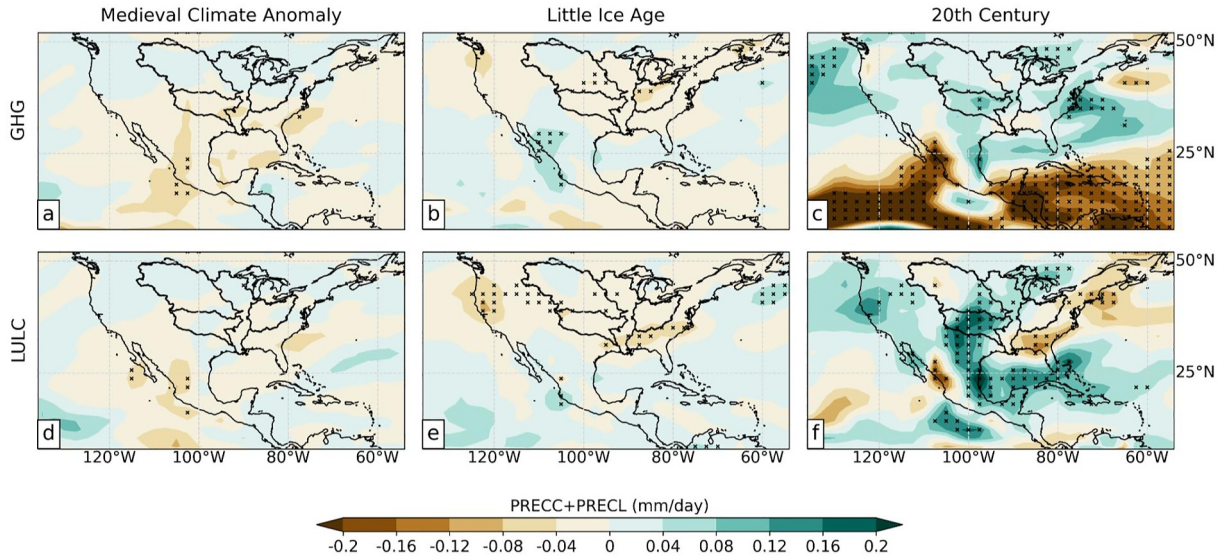

Figure 5. Comparison of CESM-LME GHG and LULC ensemble averages minus control run for **precipitation (mm/day)** in the MCA, LIA, and 20th century. Panels: Difference maps for GHG-only and control (a–c). Difference maps for LULC-only and control (d–f). The brown color represents a decrease in rainfall (drier), while the blue represents an increase (wetter). Hatched regions indicate a statistically significant difference at the 95% confidence level.

To further analyze the spatial changes in hydroclimate between the PI, 20th, and 21st centuries, we again looked at the mapped differences in hydroclimate over the MRB. In the 21st century, the basin is projected to be drier than the PI and the 20th century. Evapotranspiration increases while soil moisture, snow melt, and runoff decrease (Figure 16). The Ohio River basin alone experiences a 5% increase in runoff in the 21st century compared to the 20th century. However, the largest regionally-averaged change in runoff is a 23% decrease over the Arkansas-White River basin (Figure 16b). The largest regionally-averaged increases in evapotranspiration are seen over the Upper MRB, Missouri River, and Ohio River basins (Figure 16c). Snow melt decreases by more than 20% over the Upper MRB and Missouri River basin and by more than 40% over the Lower MRB, Arkansas-White

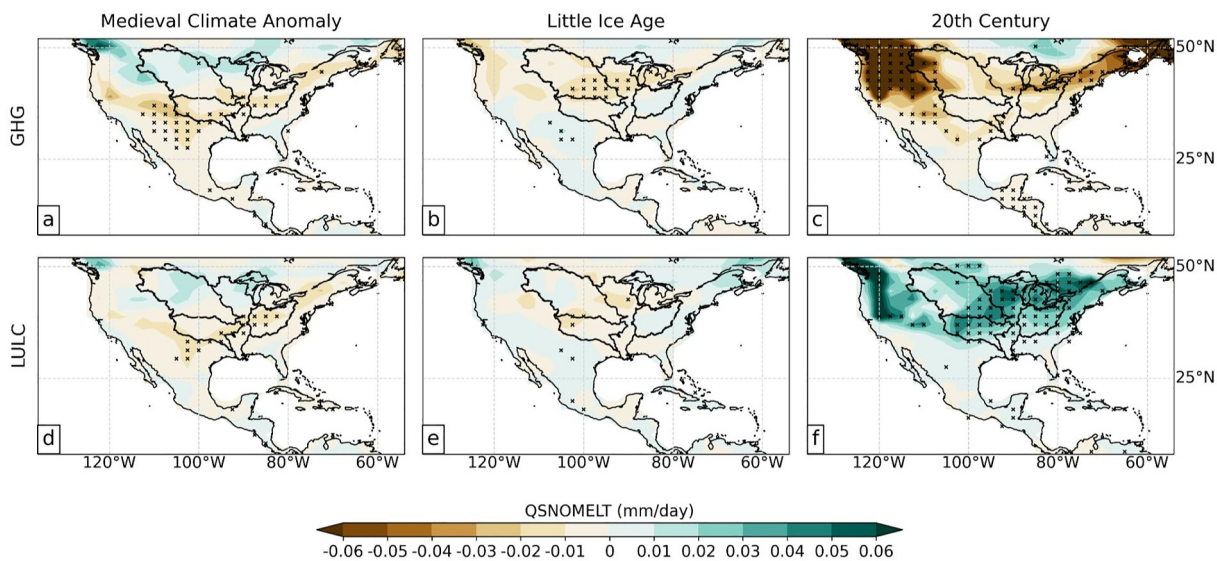

Figure 6. Comparison of CESM-LME GHG and LULC ensemble averages minus control run for **snow melt (mm/day)** in the MCA, LIA, and 20th century. Panels: Difference maps for GHG-only and control (a–c). Difference maps for LULC-only and control (d–f). The brown color represents a decrease in snow melt (drier), while the blue represents an increase (wetter). Hatched regions indicate a statistically significant difference at the 95% confidence level.

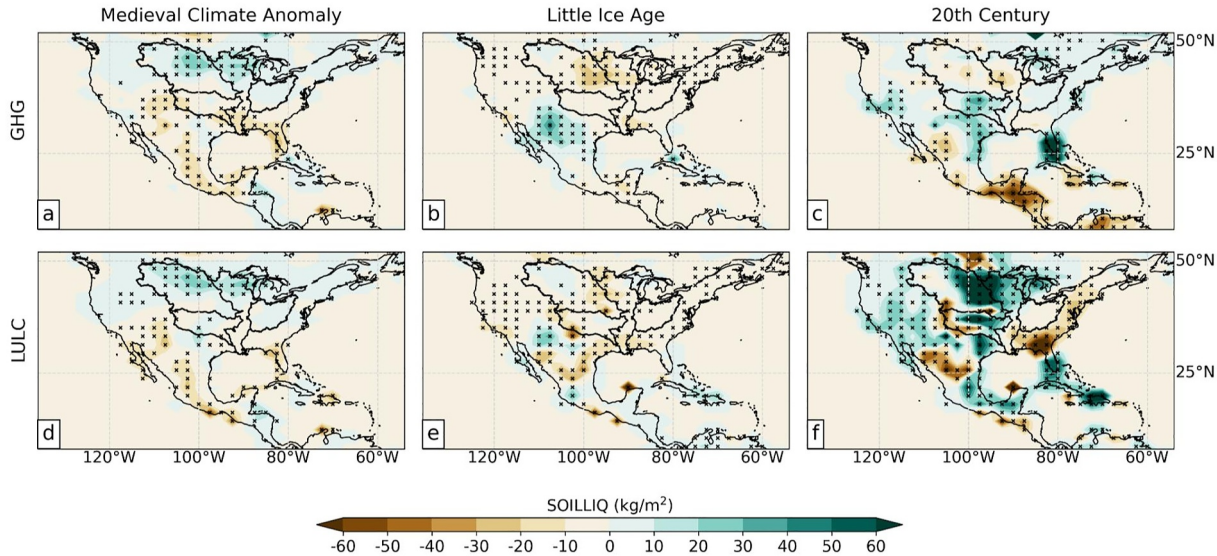

Figure 7. Comparison of CESM-LME GHG and LULC ensemble averages minus control run for **soil moisture** (kg/m^2) in the MCA, LIA, and 20th century. Panels: Difference maps for GHG-only and control (a–c). Difference maps for LULC-only and control (d–f). The brown color represents a decrease in soil moisture (drier), while the blue represents an increase (wetter). Hatched regions indicate a statistically significant difference at the 95% confidence level.

River, and Ohio River basins (Figure 16e). Despite the overall drying trend, precipitation is projected to significantly increase over all tributary basins, excluding the Arkansas-White River basin, during the 21st century compared to the 20th century. Precipitation increases by approximately 7%–10% over the Upper MRB, Missouri River, and Ohio River basins from the 20th to 21st century (Figure 16d). Under full forcing, most of the basin exhibits statistically significant shifts toward drier conditions (i.e., increased evapotranspiration and decreased soil moisture, snow melt, and runoff) in the 21st century compared to the 20th century. Finally, the differences in the hydroclimate variables between the PI and 21st century (Figure 17) are very similar to those seen in Figure 16 (which shows the percent change for the 21st vs. the 20th century).

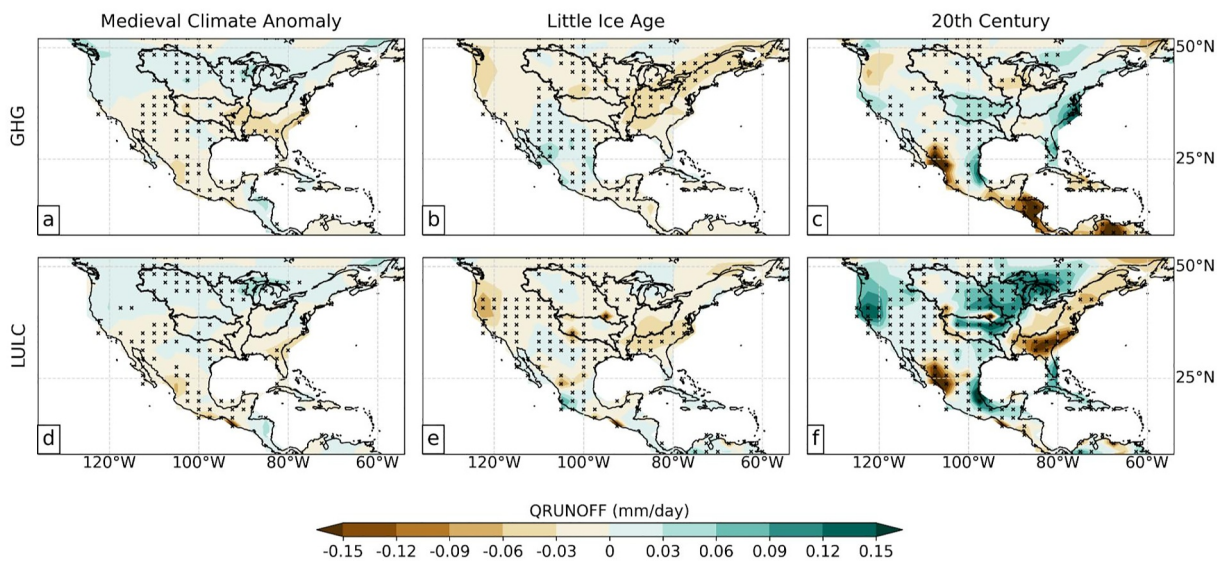

Figure 8. Comparison of CESM-LME GHG and LULC ensemble averages minus control run for **runoff** (mm/day) in the MCA, LIA, and 20th century. Panels: Difference maps for GHG-only and control (a–c). Difference maps for LULC-only and control (d–f). The brown color represents a decrease in runoff (drier), while the blue represents an increase (wetter). Hatched regions indicate a statistically significant difference at the 95% confidence level.

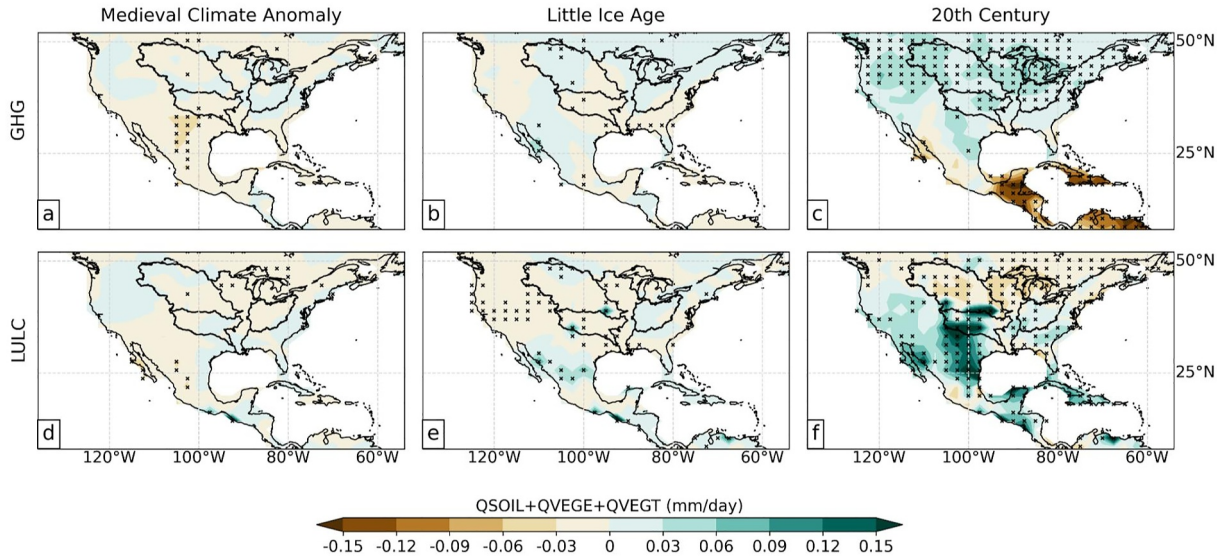

Figure 9. Comparison of CESM-LME GHG and LULC ensemble averages minus control run for **evapotranspiration (mm/day)** in the MCA, LIA, and 20th century. Panels: Difference maps for GHG-only and control (a–c). Difference maps for LULC-only and control (d–f). The brown color represents a decrease in evapotranspiration (wetter), while the blue represents an increase (drier). Hatched regions indicate a statistically significant difference at the 95% confidence level.

3.3. Risk Ratio Calculations

To evaluate how hydroclimate extremes evolve over the MRB from 850 to 2000 CE, we used risk ratios to test how discharge statistics change amongst different single-forcing simulations. Table 4 compares risk ratios for the PI and 20th century. Risk ratios are reported for individual single-forcing ensembles. There is an 8% decrease in the risk ratio for GHG-only forcing from the PI to the 20th century. Therefore, the risk of extreme discharge and flooding under GHG forcing decreases in the 20th century in the lower Mississippi basin. There is no change in the calculated risk ratio for the VOLC-only ensemble. Risk ratios for both SOLAR and AER forcing experiments are also associated with a lower risk of extreme discharge (Table S2 in Supporting Information S1). Under LULC forcing, there is a 44% increase in the risk ratio for the 20th century compared to the PI, indicating an increase in risk of extreme discharge due to LULC changes alone.

3.4. Annual Exceedance Probabilities

Calculating annual exceedance probabilities (or flood frequency analysis, FFA) facilitates a critical evaluation of the distribution of extreme discharges under different forcing scenarios in the LME. We use annual maximum discharge data from all single- and full-forcing ensemble members, and assume stationarity for the FFA; put another way, we focus only on the change in distribution of peak flows across different forcing scenarios. Figure 18 explores these changes at Vicksburg, Mississippi in the Lower MRB. The magnitudes of discharge in the upper end of each distribution (e.g., values with a 5, 2, 1, or 0.5% chance of occurrence in any given year) shown in the inset of Figure 18 are the highest in the full-forcing simulations, and lowest in the GHG- and AER-only simulations. Across all annual exceedance probabilities, peak annual discharge from the GHG and AER single-forcing simulations are lower compared to the other forcings, indicating that the Lower MRB experiences drier conditions under GHG and AER forcing (Figure 18 and Figure S15 in Supporting Information S1). This, along with the risk ratio results (Table 4 and Table S2 in Supporting Information S1), suggests GHG and AER forcing are responsible for a decrease in discharge, and therefore drier conditions, from the PI to the 20th century. However, the full-forcing ensemble in Figures 12a–12e shows that the MRB is generally wetter in the 20th century compared to the PI. Figure 18 supports the interpretation that LULC forcing contributes to wetter conditions in the ensemble, and higher peak discharge in the tails of the distribution (*sim* above the 95th percentile). While not anthropogenic, we additionally note that the VOLC-only simulations also show larger discharge values for peak exceedance probabilities, consistent with Figure 11 (see Section 3.1). We conclude from Figure 18 that

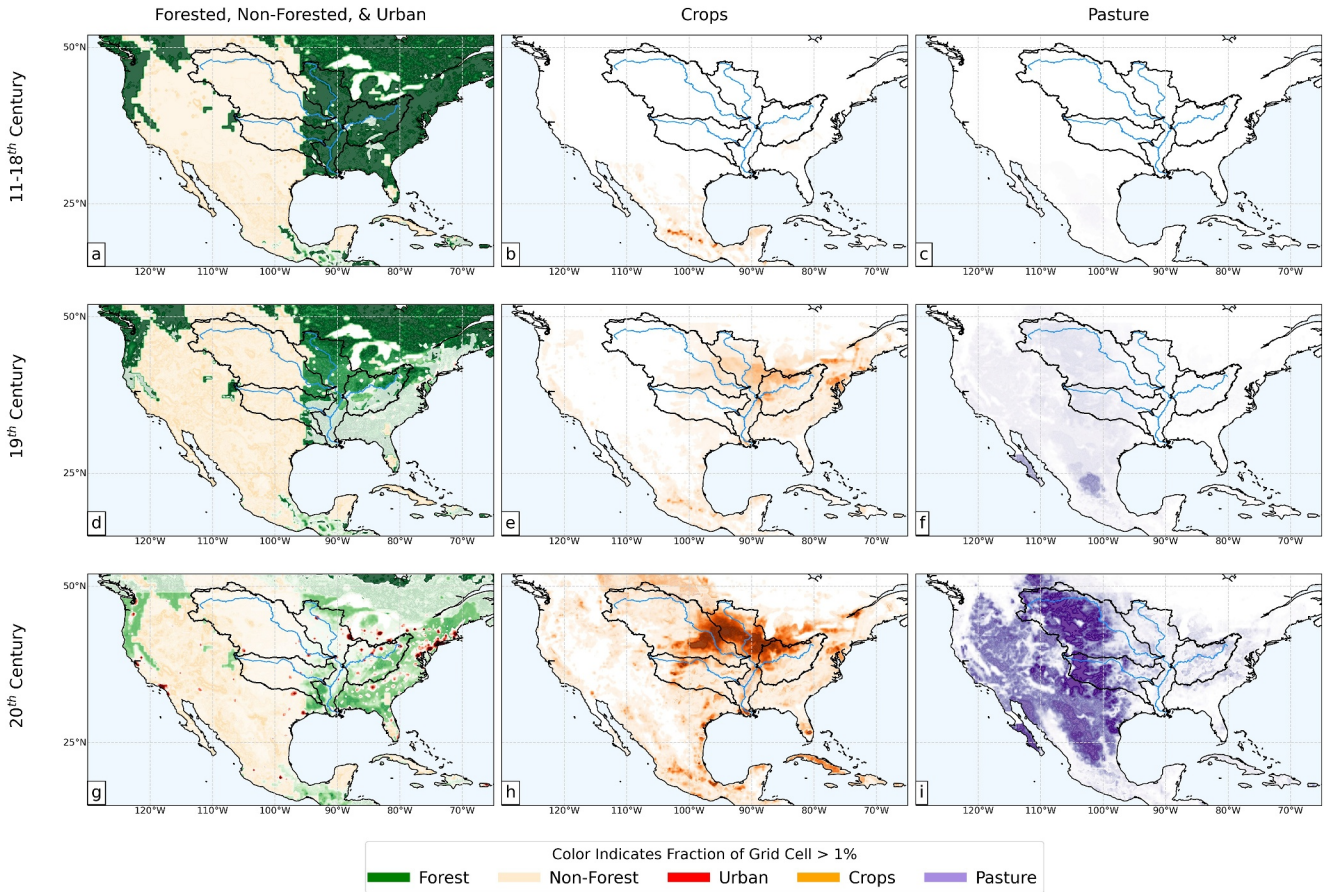

Figure 10. Evolution of land use over the continental United States from the 11th to 20th century (units are "fraction of grid cell"). Twelve "states of land use" variables from the LUH2 v2h data set are divided into subgroups (forested, non-forested, urban, crops, and pasture). Panels: Land use types are averaged from the 11th to 18th century given negligible changes in land use before the 19th century (a–c). We then compare these averages to land use during the 19th (d–f) and 20th centuries (g–i). Overall, both forested and non-forested land have decreased over time, while crops, pasture, and urban land have increased.

GHG forcing was not the main driver behind the changes seen in the simulated peak annual discharge for the 20th century: rather, LULC forcing plays a larger role (suggesting possible mitigation pathways).

4. Discussion and Conclusions

Changes in the frequency and severity of recent floods and low-flow events on the Mississippi River necessitate a renewed focus on how anthropogenic climate change will alter hydroclimate risks in the basin. To enhance projections of flood and drought conditions, we here focused on characterizing the hydroclimate drivers of large-scale changes in river discharge within controlled model simulation experiments spanning 850–2100 CE. Specifically, this work capitalizes on the CESM-LME single-forcing simulations to identify the hydroclimatic mechanisms driving changes in MRB discharge in the past and present to better diagnose how hydroclimate risks will evolve in the future. Our study interrogates three key questions surrounding how discharge evolves over the LM, the hydroclimatic mechanisms and external forcings driving those changes, and the individual tributary contributions and spatial heterogeneity of discharge fluxes across the full MRB.

First, we examined how river discharge responds to individual external climate forcings (GHG, LULC, VOLC, AER, SOLAR) over the LM. We highlighted significant shifts in discharge under FULL, GHG, and LULC forcing during the 20th century compared to the MCA and LIA (Figures 2–4 and Table 1). Changes in 20th century river discharge in response to LULC forcing are more significant than that in the GHG simulations for many of the tributaries (Table 1). We further evaluated the spatial hydroclimate pattern responses of precipitation, snow melt, soil moisture, runoff, and evapotranspiration to each external climate forcing by subtracting the CESM-LME control run from the single-forcing ensembles. Under GHG forcing, runoff decreases across the

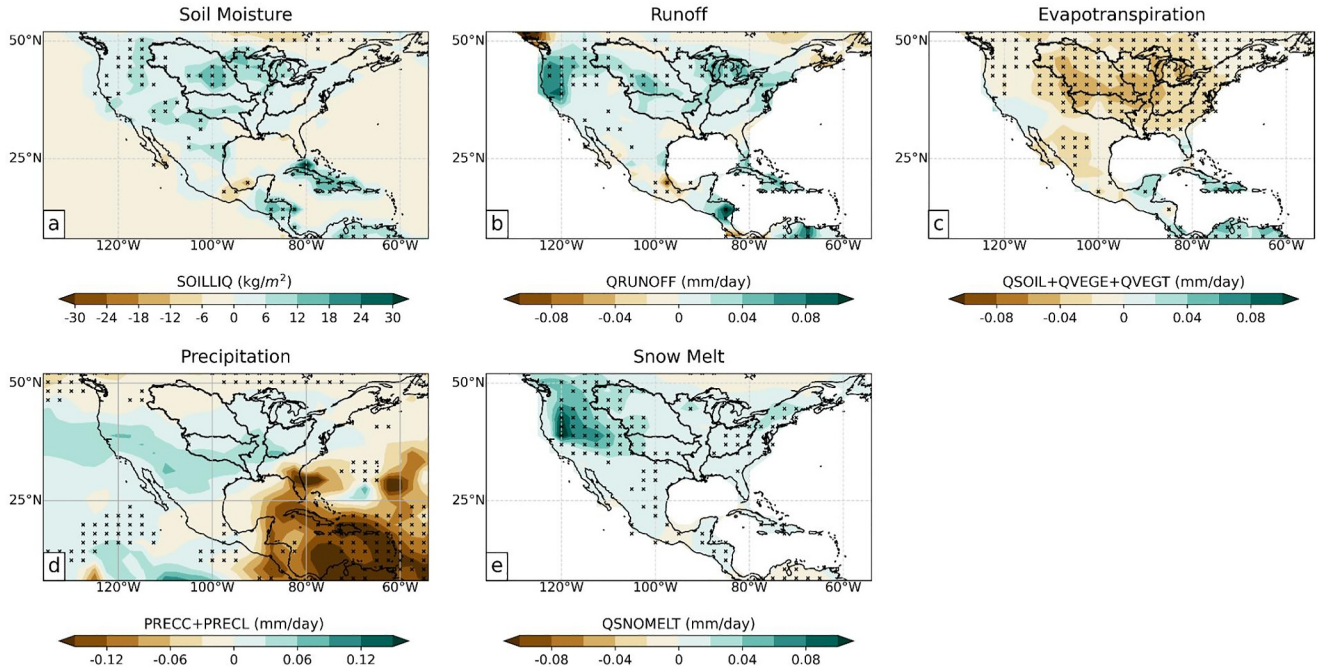

Figure 11. CESM-LME ensemble averages eruption years minus non-eruption years for soil moisture (kg/m^2), runoff (mm/day), evapotranspiration (mm/day), precipitation (mm/day), and snow melt (mm/day) under **VOLC-only forcing** (a–e). Hatched regions indicate a statistically significant difference at the 95% confidence level.

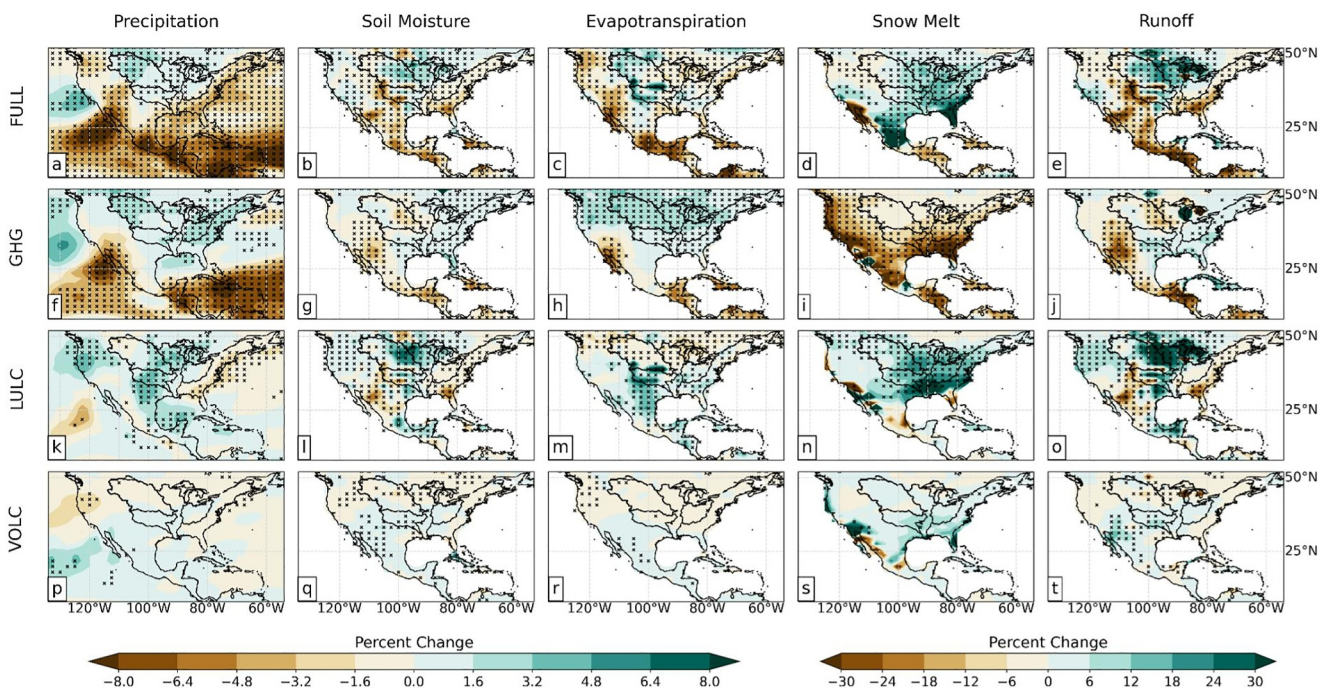

Figure 12. Percent change of CESM-LME ensemble averages from the PI to the 20th century for precipitation, soil moisture, runoff, snow melt, and evapotranspiration under four different forcing scenarios. Panels: Full (a–e), GHG (f–j), LULC (k–o), and VOLC (p–t). The percent change in the precipitation, soil moisture, and evapotranspiration variables are smaller relative to the percent changes seen in the snow melt and runoff variables, so two separate color bars are used to account for the different ranges, separated by a dashed line. Hatched regions indicate a statistically significant difference at the 95% confidence level.

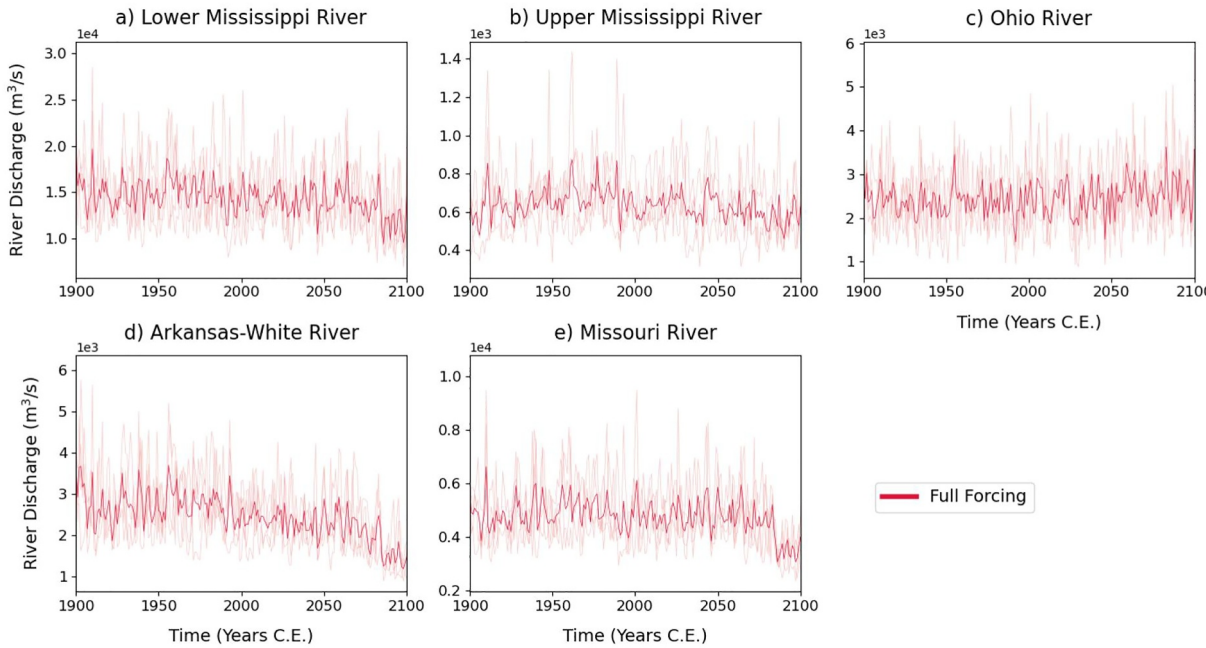

Figure 13. Time series for annual discharge (m^3/s) from one grid cell in the (a) Lower Mississippi (32.25°N, 91.25°W), (b) Upper Mississippi (43.75°N, 91.25°W), (c) Ohio River (38.25°N, 86.25°W), (d) Arkansas-White River (34.75°N, 92.25°W), and (e) Missouri River (38.75°N, 91.25°W) basin for full-forcing extension simulations 2,3,8, and 9 during the 20th and 21st centuries. Individual ensemble members are plotted as light red lines. The dark red line indicates the average of the four full-forcing simulations. Panels: Lower Mississippi River Basin (MRB) (a), Upper MRB (b), Ohio River basin (c), Arkansas-White River basin (d), and Missouri River basin (e).

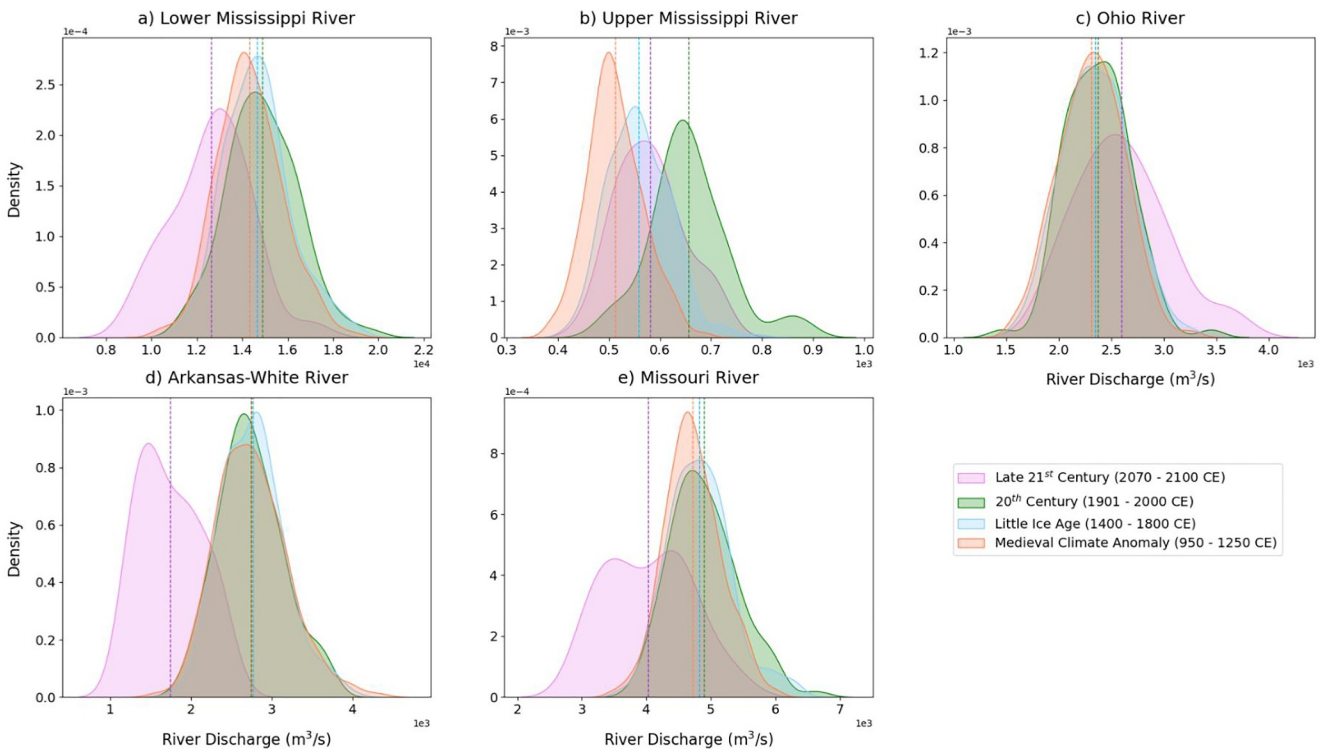

Figure 14. Probability distribution functions for annual discharge (m^3/s) from one grid cell in the (a) Lower Mississippi (32.25°N, 91.25°W), (b) Upper Mississippi (43.75°N, 91.25°W), (c) Ohio River (38.25°N, 86.25°W), (d) Arkansas-White River (34.75°N, 92.25°W), and (e) Missouri River (38.75°N, 91.25°W) basin for full-forcing extension simulations 2,3,8, and 9 during the MCA, LIA, 20th century, and 21st century. Dashed vertical lines indicate distribution means.

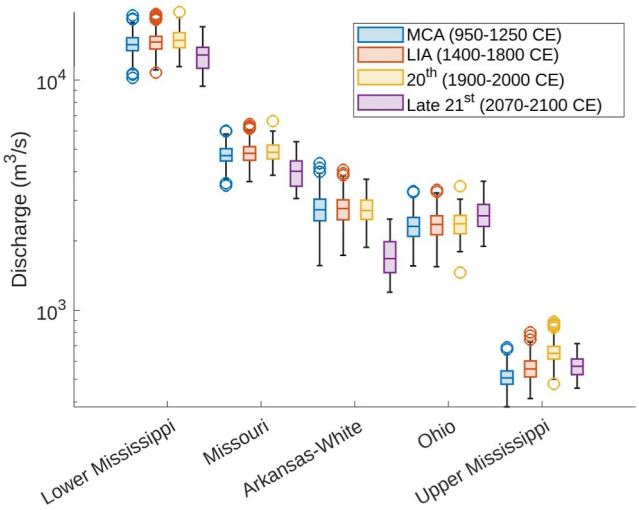

Figure 15. Box plots showing the distribution of ensemble averaged annual discharge (m^3/s) from one grid cell in the (a) Lower Mississippi (32.25°N, 91.25°W), (b) Upper Mississippi (43.75°N, 91.25°W), (c) Ohio River (38.25°N, 86.25°W), (d) Arkansas-White River (34.75°N, 92.25°W), and (e) Missouri River (38.75°N, 91.25°W) basin for the full-forcing extension simulations during the MCA, LIA, 20th century, and 21st century. The *y*-axis is represented in logarithmic scale.

Upper MRB, but increases over the Arkansas-White River and Ohio River basins (Figure 8c) alongside increased precipitation (Figure 5c) during the 20th century. Thus, the Arkansas-White River and Ohio River basins exhibit slightly wetter conditions (i.e., increased runoff and precipitation) in response to GHG-only forcing. In contrast, runoff strongly increases in large regions of the Missouri, Arkansas-White River, and Upper MRB under LULC-only forcing (Figure 8f) due to increased precipitation, snow melt, and soil moisture (Figures 5–7f) and decreased evapotranspiration (Figure 9f) during the 20th century. We acknowledge that snow melt and soil moisture are not independent forcings on runoff, but are complex components of precipitation and its balance with evapotranspiration, infiltration, and runoff. The MRB exhibits overall wetter conditions (i.e., increased runoff, precipitation, snow melt, soil moisture and decreased evapotranspiration) in response to LULC-only forcing, and the magnitude of this hydroclimate shift is larger than those simulated in the GHG-only runs (Figures 5–9c,f). Although AER-only forcing contributes to drier conditions in other regions of the MRB, namely the Lower MRB, it likely plays a role in the wettening of the Missouri River basin in the 20th century. Finally, in agreement with previous studies (D'Arrigo et al., 2013; Stevenson et al., 2016, 2018; Tejedor et al., 2021b), CESM simulates slightly wetter conditions (i.e., increased runoff, precipitation, snow melt, soil moisture and decreased evapotranspiration) across the entire basin during volcanic eruptions years (Figure 11).

The details of the LUH2 data set employed for LULC forcings in the model simulations facilitate a deeper investigation of changes in land use types that drive hydroclimate shifts in the MRB. Mass deforestation began in the Ohio River and Lower MRB basin around the start of the 19th century, but there were efforts to reforest the land toward the end of the 19th century (Figure 10g and Figures S12a and S12c in Supporting Information S1). This reforestation and the introduction of crops appears to have led to a decrease in simulated runoff and ultimately drier conditions over the Ohio compared to the other basins during the 20th century (Figure 8f). Before 1850 CE, the majority of the Missouri River and Arkansas-White River basins consisted of non-forested primary land, but the area was converted to range and crop land by the start of the 20th century (Figures 10h and 10i and Figures S12d and S12e in Supporting Information S1). The evolution from non-forested to range land may explain the increase in runoff and overall wetter conditions seen in the LULC-only simulations (Figure 8f).

We additionally examined changes in hydroclimate variables with all external forcings applied (FULL) during the PI, 20th century, and 21st century across the entire MRB. Differences (20th century minus PI) in CESM-LME ensemble averages (Figures 12a–12e) indicate a wetter 20th century compared to PI in the MRB. LULC forcing exerts the largest influence on changes in snow melt, soil moisture, and runoff (Figures 12l,n,o); all three of these variables shift toward wetter conditions in the MRB during the 20th century. Increased soil moisture over a large part of the MRB is broadly consistent with earlier studies comparing reconstructed PDSI in NADA to model PDSI (Otto-Bliesner et al., 2016, Figure 10), though the hydroclimatic response in the CESM-LME is of a lower magnitude compared to NADA (Stevenson et al., 2016; Tejedor et al., 2021a). As shown in Figure 12, the spatial patterns in the full-forcing simulations closely resemble those found in the LULC forcing simulations, with the exception of precipitation, which is similar to both GHG and LULC forcing. Risk ratios and flood frequency analyses were also computed to quantify how discharge responds to each individual forcing (Sections 3.3 and 3.4). GHG forcing leads to reduced discharge (i.e., drier conditions), while LULC forcing leads to increased discharge (i.e., wetter conditions). In other words, the CESM-LME simulations support the interpretation that 20th century changes in LULC have increased the risk of flooding in the MRB. Finally, we examined CESM-LME 21st century extension projections of

Table 3
Significance Testing for Full-Forcing Extension Distributions

		Late 21st century compared to MCA, LIA, and 20th century		
		21st, MCA	21st, LIA	21st, 20th
Full	Lower Mississippi	**D**	**D**	**D**
	Upper Mississippi	**W**	W	**D**
	Ohio	**W**	**W**	**W**
	Arkansas-White	**D**	**D**	**D**
	Missouri	**D**	**D**	**D**

Note. Each column represents a comparison between two different time periods (e.g., Late 21st century compared to MCA). Brown "D" indicates there is lower discharge in the Late 21st century and blue "W" represents higher river discharge in the Late 21st century. Bold, underlined letters indicate a statistically significant change at the 95% confidence level.

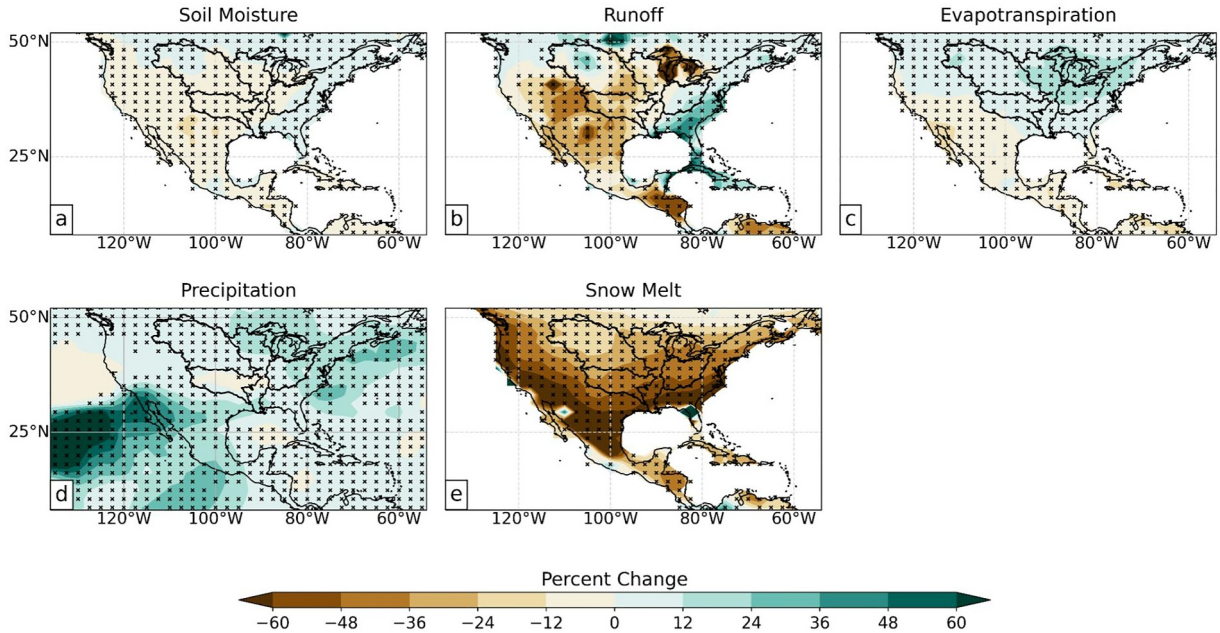

Figure 16. Hydroclimate variable percent changes for the CESM-LME ensemble average from the 20th to 21st century [(21st minus 20th)/20th]. Panels: Soil moisture (a), runoff (b), evapotranspiration (c), precipitation (d), and snow melt (e) under full-forcing extension simulations 2,3,8, and 9. Hatched regions indicate a statistically significant difference at the 95% confidence level.

discharge (FULL-only, Figure 13) and other hydroclimate variables (Figures 16 and 17). Discharge is projected to decrease in all basins except for the Ohio River basin during the late 21st century (Figures 13–15). Interestingly, while precipitation increases in the 21st century compared to the 20th century and PI (Figures 16–17d), drier conditions emerge overall. That is, reductions in runoff and snow melt and an increase in evapotranspiration all lead to an overall drying response in the MRB during the 21st century (Figures 16–17b,c,e). Simulated differences

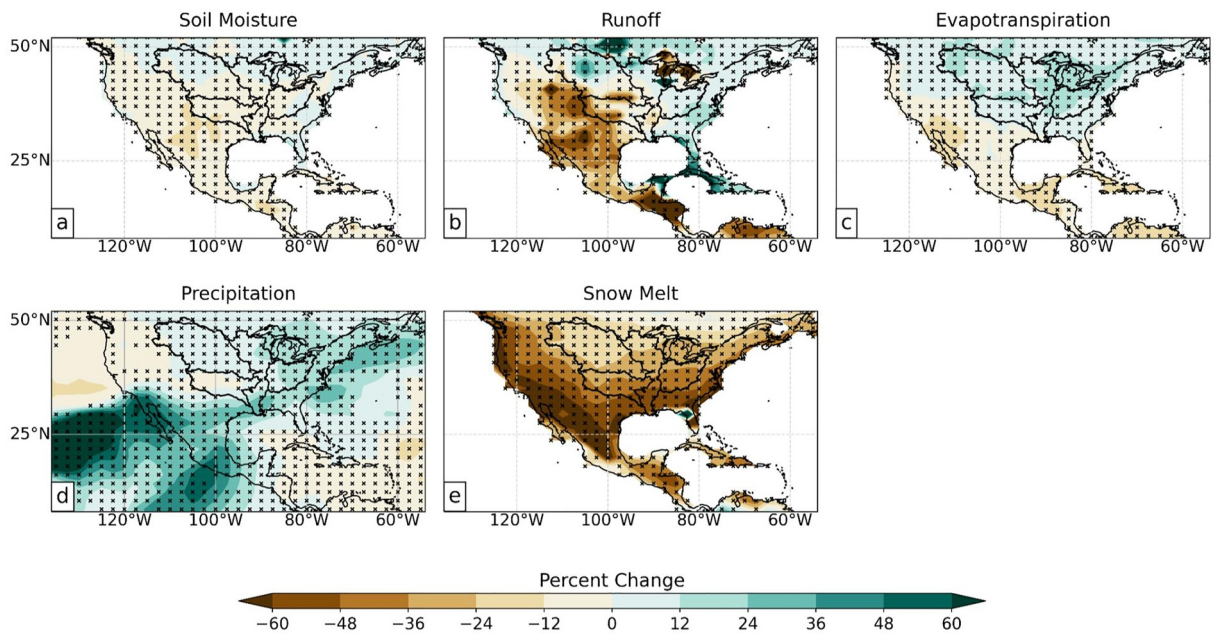

Figure 17. Hydroclimate variable percent changes for the CESM-LME ensemble average from the Pre-Industrial (PI) to the 21st century [(21st minus PI)/PI]. Panels: Soil moisture (a), runoff (b), evapotranspiration (c), precipitation (d), and snow melt (e) under full-forcing extension simulations 2,3,8, and 9. Hatched regions indicate a statistically significant difference at the 95% confidence level.

Table 4
Risk Ratios for the Pre-Industrial (850–1849 CE) and 20th Century (1901–2000 CE) for Single-Forcing Simulations GHG, LULC, and VOLC

Risk ratios		
Single-forcing	Pre-industrial (850–1849 CE)	20th century (1901–2000 CE)
GHG	0.90	0.83
LULC	0.90	1.3
VOLC	0.96	0.96

Note. Risk ratios are defined as the frequency with which single-forcing exceeds the 95th percentile of all discharge values in all full-forcing ensemble members, divided by the frequency with which full forcing exceeds the same threshold.

in soil moisture are less pronounced, but shift toward drier conditions as well (Figures 16–17a). The Ohio River shows a slight increase in runoff during the 21st century driven primarily by increased precipitation (Figures 16–17b).

Our results harbor several key findings relevant to hydroclimate hazard characterization in the MRB. Human alterations of the landscape in the MRB, captured in the LULC forcing ensemble, drive wetter conditions across the basin. Greenhouse gas forcing has been shown to increase extreme rainfall and potentially enhance flooding risk (Dunne et al., 2022), yet when compared to a LM baseline, it appears that GHG forcing may actually yield drier conditions overall. FFA underscores a substantial reduction in discharge for the highest recurrence intervals under GHG forcing, but a large increase under LULC and FULL forcing (Figure 18). These results, while limited to a single climate model ensemble, support the interpretation that human alterations to LULC have large and measurable impacts on flood risk. Two extensions of this include (a) human decision-making surrounding land

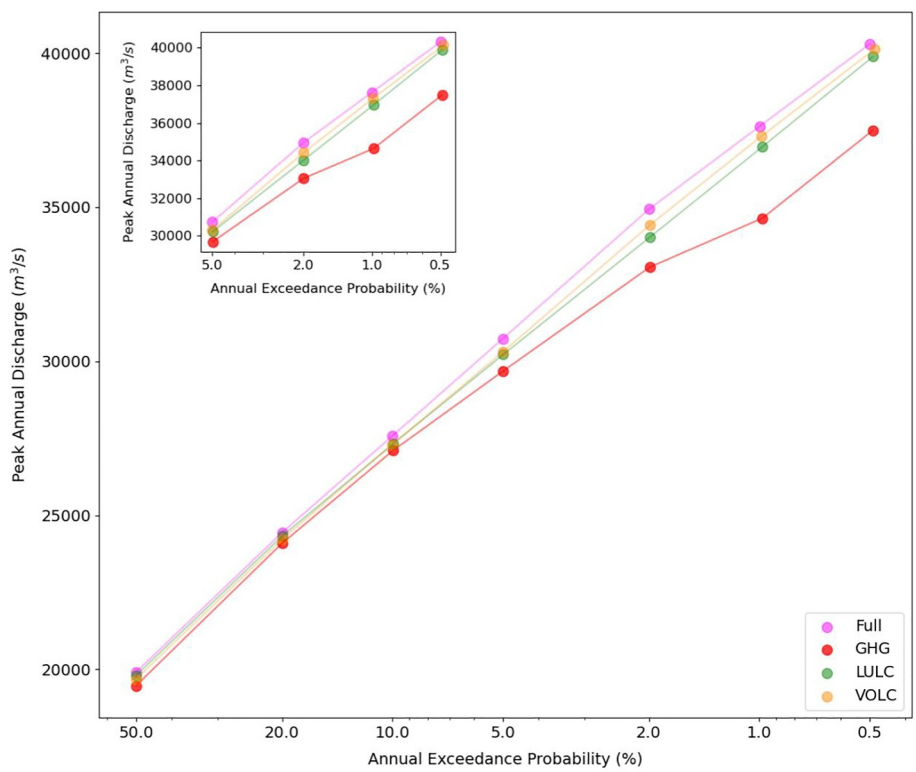

Figure 18. Annual exceedance probabilities in relation to simulated peak annual discharge at Vicksburg, Mississippi, used to compare the relative changes between different forcing scenarios (Full, GHG, LULC, and VOLC) during the Last Millennium (850–2005 CE). The inset on the top left is zoomed in on simulated peak annual discharge values with a 5, 2, 1, or 0.5% chance of occurrence in any given year.

use could prove critical to flood mitigation on short timescales, and (b) accurate representation of land surface types and changes in climate models is critical to flood hazard projections. Furthermore, greenhouse gas forcing, particularly from CO_2 emissions, will cause hundreds of years of committed atmospheric warming, accompanied by a set of consistent hydroclimate responses simulated here for the majority of the MRB (drying driven by enhanced evapotranspiration, reduced snow melt, and reduced soil moisture). These changes will evolve over decades, whereas LULC changes could impact flood risk rapidly (within months). Even far-afield changes in LULC (e.g., tropical deforestation) have been shown to affect MRB hydroclimate (Werth & Avissar, 2002). Thus, human decision-making surrounding land cover and flood infrastructure may prove to be the most important uncertainty in future flood risk. This work, aimed at generating understanding of how large-scale hydroclimate evolves across the major tributaries (e.g., projected drying in the Missouri compared to increased precipitation over the Ohio), must inform geographically targeted land use decision making in each sub-basin independently.

This research also provides important context for previous work surrounding the relative importance of climate change (i.e., GHG forcing) versus land use change and river engineering (i.e., LULC) for flood risk in global river basins. The impacts of climate change (Jha et al., 2004; Qian et al., 2007; Rossi et al., 2009), LULC (Schilling et al., 2008, 2010; Tran & O'Neill, 2013), and river engineering (Munoz et al., 2018; Pinter & Heine, 2005) all compound in reality and jointly affect changes in observed MRB discharge (Foley et al., 2004; Frans et al., 2013; Mishra et al., 2010; Pinter et al., 2008; St. George, 2018). However, various studies differ widely in their assertions of which of these matters most: for example, Pinter et al. (2008) suggested a dominant influence of infrastructure over *both* climate change and LULC forcing. Still other research (focused on the upper MRB) indicates that the increases in runoff are mainly due to climate-change-induced increases in precipitation, and that LULC is more important only on smaller spatial scales (Frans et al., 2013; Milly & Dunne, 2001). Eischeid et al. (2023) suggests ocean-atmosphere interactions may be a more important control on precipitation compared to LULC changes over the central US. As mentioned above, our work broadly supports an out-sized role of LULC and local land use management in flood control, especially on short timescales. That said, GHG forcing clearly shifts the statistics of mean hydroclimate in projections spanning the next several decades (Dunne et al., 2022). Single-forcing simulations such as those analyzed here allow us to deconvolve changes in the magnitude, sign (i.e., wet vs. dry), and timescale of each forcing's influence on hydroclimate shifts.

We acknowledge important limitations of our approach. First, the coarse spatial resolution of the atmosphere and land components of the CESM-LME may lead to a bias toward lower precipitation intensity (D. Chen & Dai, 2019), as well as earlier peaks in streamflow due to an imperfect representation of snow melt, especially at higher elevations (Jin & Wen, 2012; Toure et al., 2018). We also rely on a single climate model ensemble which contains biases in its simulation of hydroclimate and river discharge; seasonal biases in the simulation of river discharge in CESM1.2 have been documented in previous work (Dunne et al., 2022; Munoz & Dee, 2017). However, our evaluation focuses on decadal-to-centennial scale shifts in hydroclimate, likely mitigating the impacts of some of these biases on the key goals of the present study. Figure S9 in Supporting Information S1 also shows that the magnitude and sign of seasonal changes from the PI to the 20th century are similar across all months. The land model hydrology in CESM1.2 (CLM4) is also quite limited: in particular, land use changes are not completely represented in models (despite their large impact, confirmed in this work). LULC factors that drive changes in runoff include baseflow, timing of snow melt, and percentage of pasture and cropland (Knox, 2001; Schilling et al., 2010; Twine et al., 2004; Zhang & Schilling, 2006); errors in the representation of these key surface variables are likely to have a large impact on CESM's simulation of surface hydrology. In addition, the non-stationary parameterization of flow velocity in the CESM boundary condition files likely biases runoff over land. Flow velocities in CESM1 RTM simulations are dependent on mean topographic slope and do not consider roughness coefficients (Oleson et al., 2013) despite land use changes over time, which affects surface water flows. In addition, human modulations to the river basin, from engineering infrastructure to irrigation, are not included in the CESM-LME simulations. We speculate that the inclusion of irrigation might result in cooler surface temperatures (L. Chen & Dirmeyer, 2019), increased evapotranspiration and regional differences in precipitation (Thiery et al., 2017; Zeng et al., 2017). With irrigation turned on, we might expect decreased river discharge in some regions (Biemans et al., 2011), but due to the complexity of groundwater and streamflow interactions over the basin, it is unclear exactly how irrigation might impact river discharge. Broadly speaking, additional research using a multi-model ensemble and spanning a range of hydraulic modeling complexities would be required to further reduce such uncertainties (e.g., connecting large-scale hydroclimate changes from GCMs to computational hydrology at finer scales). Such efforts are ongoing amongst the authors of this work.

Finally, extension research must consider variations in natural climate modes, such as the Bermuda High, North Atlantic Oscillation, Atlantic Multi-Decadal Oscillation (AMO), and the El Niño-Southern Oscillation (ENSO), which will compound with anthropogenic climate change to alter hydroclimate across the MRB in the 21st century. The AMO may have less impact on the MRB than previously thought (Luo et al., 2022), while ENSO heavily modulates interannual flood risk in the basin (Luo et al., 2022, 2023; Munoz & Dee, 2017; Munoz et al., 2018). An additional caveat of the CESM is that it tends to inflate ENSO variance (Muñoz et al., 2023; Stevenson et al., 2016). Characterizing how interannual and multidecadal modes of internal variability modulate hydroclimate risks amidst persistent anthropogenic forcing is critical for both seasonal-to-decadal climate prediction and accurate engineering design of flood control structures.

In closing, climate change has and will continue to alter the MRB's flow regimes as well as the magnitude and frequency of extreme flooding events in the MRB (Lewis et al., 2023). Understanding how naturally occurring variations in the climate system, in addition to anthropogenic activity, independently influence climate change can help mitigate future risk in the 21st century. Identifying how various external forcings like GHG and LULC, both tightly coupled to human decisions, will alter hydroclimate and future flooding hazard must guide government agencies (e.g., Army Corps of Engineers) toward informed decisions about MR&T project updates and regional flood mitigation strategies, saving lives and money in the process. This work takes an additional step toward understanding the drivers of changes in U.S. hydroclimate in the 21st century by using the past as prologue for future risk.

Data Availability Statement

Climate model data from CESM was downloaded via the Earth System Grid earthsystemgrid.org and the CESM-LME forcing files may be found at https://www.cesm.ucar.edu/community-projects/lme/instructions. All of the data sets used in this analysis are publicly available: CESM LME Atmosphere (https://www.earthsystemgrid.org/dataset/ucar.cgd.ccsm4.cesmLME.atm.proc.monthly_ave.html), Land (https://www.earthsystemgrid.org/dataset/ucar.cgd.ccsm4.cesmLME.lnd.proc.monthly_ave.html), and River (https://www.earthsystemgrid.org/dataset/ucar.cgd.ccsm4.cesmLME.rof.proc.monthly_ave.html) (Kay et al., 2015; Otto-Bliesner et al., 2016), ECMWF ERA5 (Hersbach et al., 2020, 2023), GPCC (https://iridl.ldeo.columbia.edu/SOURCES/.WCRP/.GCOS/.GPCC/.FDP/.version2018/.2p5/.prcp/datafiles.html) (Becker et al., 2013; Schneider et al., 2017). The USGS water data and streamgage locations are available at https://waterdata.usgs.gov/nwis/. The documentation for the river routing model may be found at https://www2.cesm.ucar.edu/models/cesm1.2/rtm/ (Branstetter, 2001; Branstetter & Famiglietti, 1999). The Land Use Harmonization^2 historical data set was downloaded at https://luh.umd.edu/data.shtml (G. Hurtt et al., 2019; G. C. Hurtt et al., 2020).

Acknowledgments
This research was funded by the National Science Foundation and was accomplished under Grants CLD-2147781 (Dee, Doss-Gollin), CLD-2147782 (Muñoz), and EAR-1804107 (Muñoz). This work was also supported by the Ken Kennedy Institute Computational Science and Engineering Recruiting Fellowship, funded by the Energy HPC Conference.

References

Amorim, R., Villarini, G., Veacth, W., & White, K. (2023). Reduced and more fragmented Mississippi River navigability by rising flow. *Geophysical Research Letters*, *50*(19), e2023GL104619. https://doi.org/10.1029/2023gl104619

Arcement, G. J., & Schneider, V. R. (1989). Guide for selecting Manning's roughness coefficients for natural channels and flood plains. https://doi.org/10.3133/wsp2339

Assessing the U.S. Climate in October 2022. (2022). Drought extends across nearly two-thirds of the Lower 48; Mississippi River at lowest water levels in a decade. Retrieved from https://www.ncei.noaa.gov/news/national-climate-202210

Atwood, A. R., Battisti, D., Wu, E., Frierson, D., & Sachs, J. P. (2021). Data-model comparisons of tropical hydroclimate changes over the common era. *Paleoceanography and Paleoclimatology*, *36*(7), e2020PA003934. https://doi.org/10.1029/2020pa003934

Batker, D., Mack, S. K., Sklar, F. H., Nuttle, W. K., Kelly, M. E., & Freeman, A. M. (2014). The importance of Mississippi delta restoration on the local and national economies. In *Perspectives on the restoration of the Mississippi Delta: The once and future delta* (pp. 141–153).

Becker, A., Finger, P., Meyer-Christoffer, A., Rudolf, B., Schamm, K., Schneider, U., & Ziese, M. (2013). A description of the global land-surface precipitation data products of the global precipitation climatology centre with sample applications including centennial (trend) analysis from 1901–present. *Earth System Science Data*, *5*(1), 71–99. https://doi.org/10.5194/essd-5-71-2013

Bhattacharya, T., & Coats, S. (2020). Atlantic-Pacific gradients drive last millennium hydroclimate variability in Mesoamerica. *Geophysical Research Letters*, *47*(13), e2020GL088061. https://doi.org/10.1029/2020gl088061

Biemans, H., Haddeland, I., Kabat, P., Ludwig, F., Hutjes, R. W., Heinke, J., et al. (2011). Impact of reservoirs on river discharge and irrigation water supply during the 20th century. *Water Resources Research*, *47*(3). https://doi.org/10.1029/2009wr008929

Bonan, G. B. (2008). Forests and climate change: Forcings, feedbacks, and the climate benefits of forests. *Science*, *320*(5882), 1444–1449. https://doi.org/10.1126/science.1155121

Branstetter, M. L. (2001). *Development of a parallel river transport algorithm and applications to climate studies*. The University of Texas at Austin. Retrieved from http://hdl.handle.net/2152/10545

Branstetter, M. L., & Famiglietti, J. S. (1999). Testing the sensitivity of GCM-simulated runoff to climate model resolution using a parallel river transport algorithm. In *Preprints, 14th conference on hydrology* (pp. 391–392). American Meteorological Society.

Chen, D., & Dai, A. (2019). Precipitation characteristics in the community atmosphere model and their dependence on model physics and resolution. *Journal of Advances in Modeling Earth Systems*, *11*(7), 2352–2374. https://doi.org/10.1029/2018ms001536
Chen, L., & Dirmeyer, P. A. (2019). Global observed and modelled impacts of irrigation on surface temperature. *International Journal of Climatology*, *39*(5), 2587–2600. https://doi.org/10.1002/joc.5973
Chen, L., & Dirmeyer, P. A. (2020). Reconciling the disagreement between observed and simulated temperature responses to deforestation. *Nature Communications*, *11*(1), 202. https://doi.org/10.1038/s41467-019-14017-0
Cleaveland, M. K. (2000). A 963-year reconstruction of summer (JJA) stream flow in the white river, Arkansas, USA, from tree-rings. *The Holocene*, *10*(1), 33–41. https://doi.org/10.1191/095968300666157027
Cook, E. R., Seager, R., Cane, M. A., & Stahle, D. W. (2007). North American drought: Reconstructions, causes, and consequences. *Earth-Science Reviews*, *81*(1–2), 93–134. https://doi.org/10.1016/j.earscirev.2006.12.002
Cook, E. R., Seager, R., Heim Jr, R. R., Vose, R. S., Herweijer, C., & Woodhouse, C. (2010). Megadroughts in north America: Placing IPCC projections of hydroclimatic change in a long-term palaeoclimate context. *Journal of Quaternary Science*, *25*(1), 48–61. https://doi.org/10.1002/jqs.1303
Cook, E. R., Woodhouse, C. A., Eakin, C. M., Meko, D. M., & Stahle, D. W. (2004). Long-term aridity changes in the western United States. *Science*, *306*(5698), 1015–1018. https://doi.org/10.1126/science.1102586
Dai, A., & Trenberth, K. E. (2002). Estimates of freshwater discharge from continents: Latitudinal and seasonal variations. *Journal of Hydrometeorology*, *3*(6), 660–687. https://doi.org/10.1175/1525-7541(2002)003<0660:eofdfc>2.0.co;2
Danabasoglu, G., Lamarque, J.-F., Bacmeister, J., Bailey, D., DuVivier, A., Edwards, J., et al. (2020). The community earth system model version 2 (CESM2). *Journal of Advances in Modeling Earth Systems*, *12*(2), e2019MS001916. https://doi.org/10.1029/2019ms001916
D'Arrigo, R., Wilson, R., & Anchukaitis, K. J. (2013). Volcanic cooling signal in tree ring temperature records for the past millennium. *Journal of Geophysical Research: Atmospheres*, *118*(16), 9000–9010. https://doi.org/10.1002/jgrd.50692
Dee, S., Okumura, Y., Stevenson, S., & Di Nezio, P. (2020). Enhanced North American ENSO teleconnections during the Little Ice Age revealed by Paleoclimate Data Assimilation. *Geophysical Research Letters*, *47*(15), e2020GL087504. https://doi.org/10.1029/2020gl087504
Dee, S. G., & Steiger, N. J. (2022). Enso's response to volcanism in a data assimilation-based paleoclimate reconstruction over the common era. *Paleoceanography and Paleoclimatology*, *37*(3), e2021PA004290. https://doi.org/10.1029/2021pa004290
DeHaan, H., Stamper, J., & Walters, B. (2012). Mississippi river and tributaries system 2011 post-flood report: Documenting the 2011 flood, the corps' response, and the performance of the mr&t system.
Ding, B., Zhang, Y., Yu, X., Jia, G., Wang, Y., Wang, Y., et al. (2022). Effects of forest cover type and ratio changes on runoff and its components. *International Soil and Water Conservation Research*, *10*(3), 445–456. https://doi.org/10.1016/j.iswcr.2022.01.006
Dunne, K., Dee, S., Reinders, J., Muñoz, S., & Nittrouer, J. (2022). Examining the impact of emissions scenario on lower Mississippi river flood hazard projections. *Environmental Research Communications*, *4*(9), 091001. https://doi.org/10.1088/2515-7620/ac8d53
Eischeid, J., Hoerling, M., Quan, X.-W., Kumar, A., Barsugli, J., Labe, Z., et al. (2023). Why has the summertime central us warming hole not disappeared? *Journal of Climate*, *36*(20), 7319–7336. https://doi.org/10.1175/jcli-d-22-0716.1
Engman, E. T. (1986). Roughness coefficients for routing surface runoff. *Journal of Irrigation and Drainage Engineering*, *112*(1), 39–53. https://doi.org/10.1061/(asce)0733-9437(1986)112:1(39)
Fasullo, J. T., Otto-Bliesner, B. L., & Stevenson, S. (2019). The influence of volcanic aerosol meridional structure on monsoon responses over the last millennium. *Geophysical Research Letters*, *46*(21), 12350–12359. https://doi.org/10.1029/2019gl084377
Foley, J. A., Kucharik, C. J., Twine, T. E., Coe, M. T., & Donner, S. D. (2004). Land use, land cover, and climate change across the Mississippi basin: Impacts on selected land and water resources. In *Ecosystems and land use change* (Vol. 15, pp. 249–261). https://doi.org/10.1029/153gm19
Frans, C., Istanbulluoglu, E., Mishra, V., Munoz-Arriola, F., & Lettenmaier, D. P. (2013). Are climatic or land cover changes the dominant cause of runoff trends in the Upper Mississippi River Basin? *Geophysical Research Letters*, *40*(6), 1104–1110. https://doi.org/10.1002/grl.50262
Gao, C., Robock, A., & Ammann, C. (2008). Volcanic forcing of climate over the past 1500 years: An improved ice core-based index for climate models. *Journal of Geophysical Research*, *113*(D23). https://doi.org/10.1029/2008JD010239
Georgakakos, A. (2014). Ch 3: Water resources in M Melillo, Terese (TC) Richmond and GW Yohe. In *Climate change impacts in the United States: The third national climate assessment*.
Gibson, D. K., Bird, B. W., Pollard, H. J., Nealy, C. A., Barr, R. C., & Escobar, J. (2022). Using sediment accumulation rates in floodplain paleochannel lakes to reconstruct climate-flood relationships on the lower Ohio River. *Quaternary Science Reviews*, *298*, 107852. https://doi.org/10.1016/j.quascirev.2022.107852
Grove, J. (1988). The little ice age.
Hansen, J. E., & Sato, M. (2012). *Paleoclimate implications for human-made climate change*. Springer.
Hayhoe, K., Wuebbles, D. J., Easterling, D. R., Fahey, D. W., Doherty, S., Kossin, J. P., et al. (2018). Chapter 2 : Our changing climate. impacts, risks, and adaptation in the United States: The fourth national climate assessment, volume II (Tech. Rep.). https://doi.org/10.7930/nca4.2018.ch2
Held, I. M., & Soden, B. J. (2006). Robust responses of the hydrological cycle to global warming. *Journal of Climate*, *19*(21), 5686–5699. https://doi.org/10.1175/jcli3990.1
Hersbach, H., Bell, B., Berrisford, P., Biavati, G., Horányi, A., Muñoz Sabater, J., et al. (2023). ERA5 monthly averaged data on single levels from 1940 to present [dataset]. *Copernicus Climate Change Service (C3S) Climate Data Store (CDS)*. https://doi.org/10.24381/cds.f17050d7
Hersbach, H., Bell, B., Berrisford, P., Hirahara, S., Horányi, A., Muñoz-Sabater, J., et al. (2020). The ERA5 global reanalysis. *Quarterly Journal of the Royal Meteorological Society*, *146*(730), 1999–2049. https://doi.org/10.1002/qj.3803
Herweijer, C., Seager, R., & Cook, E. R. (2006). North American droughts of the mid to late nineteenth century: A history, simulation and implication for mediaeval drought. *The Holocene*, *16*(2), 159–171. https://doi.org/10.1191/0959683606hl917rp
Herweijer, C., Seager, R., Cook, E. R., & Emile-Geay, J. (2007). North American droughts of the last millennium from a gridded network of tree-ring data. *Journal of Climate*, *20*(7), 1353–1376. https://doi.org/10.1175/jcli4042.1
Hoell, A., Hoerling, M., Quan, X.-W., & Robinson, R. (2023). Recent high Missouri River Basin runoff was unlikely caused by climate change. *Journal of Applied Meteorology and Climatology*, *62*(6), 657–675. https://doi.org/10.1175/jamc-d-22-0158.1
Hoell, A., Quan, X.-W., Robinson, R., & Hoerling, M. (2024). Potential predictability of two-year droughts in the Missouri River Basin. *Journal of Climate*, *37*(12), 3413–3432. https://doi.org/10.1175/jcli-d-23-0588.1
Hurrell, J. W., Holland, M. M., Gent, P. R., Ghan, S., Kay, J. E., Kushner, P. J., et al. (2013). The community earth system model: A framework for collaborative research. *Bulletin of the American Meteorological Society*, *94*(9), 1339–1360. https://doi.org/10.1175/bams-d-12-00121.1
Hurtt, G., Chini, L., Sahajpal, R., Frolking, S., Bodirsky, B. L., Calvin, K., et al. (2019). Harmonization of global land use change and management for the period 850-2015 [Dataset]. *Earth System Grid Federation*. https://doi.org/10.22033/ESGF/input4MIPs.10454

Hurtt, G. C., Chini, L., Sahajpal, R., Frolking, S., Bodirsky, B. L., Calvin, K., et al. (2020). Harmonization of global land use change and management for the period 850–2100 (LUH2) for CMIP6. *Geoscientific Model Development*, *13*(11), 5425–5464. https://doi.org/10.5194/gmd-13-5425-2020

IPCC. (2022). Summary for policymakers [Book Section]. In H. O. Pörtner, D. C. Roberts, E. S. Poloczanska, K. Mintenbeck, M. Tignor, A. Alegría, et al. (Eds.), *Climate change 2022: Impacts, adaptation, and vulnerability. Contribution of working group ii to the sixth assessment report of the intergovernmental panel on climate change*. Cambridge University Press. (In Press).

Ivancic, T. J., & Shaw, S. B. (2016). A US-based analysis of the ability of the Clausius-Clapeyron relationship to explain changes in extreme rainfall with changing temperature. *Journal of Geophysical Research: Atmospheres*, *121*(7), 3066–3078. https://doi.org/10.1002/2015jd024288

Jha, M., Pan, Z., Takle, E. S., & Gu, R. (2004). Impacts of climate change on streamflow in the Upper Mississippi River Basin: A regional climate model perspective. *Journal of Geophysical Research*, *109*(D9). https://doi.org/10.1029/2003jd003686

Jin, J., & Wen, L. (2012). Evaluation of snowmelt simulation in the weather research and forecasting model. *Journal of Geophysical Research*, *117*(D10). https://doi.org/10.1029/2011jd016980

Jones, P. D., & Mann, M. E. (2004). Climate over past millennia. *Reviews of Geophysics*, *42*(2). https://doi.org/10.1029/2003rg000143

Kay, J. E., Deser, C., Phillips, A., Mai, A., Hannay, C., Strand, G., et al. (2015). The community earth system model (CESM) large ensemble project: A community resource for studying climate change in the presence of internal climate variability. *Bulletin of the American Meteorological Society*, *96*(8), 1333–1349. https://doi.org/10.1175/bams-d-13-00255.1

Kirchmeier-Young, M. C., Zwiers, F. W., Gillett, N. P., & Cannon, A. J. (2017). Attributing extreme fire risk in western Canada to human emissions. *Climatic Change*, *144*(2), 365–379. https://doi.org/10.1007/s10584-017-2030-0

Knox, J. C. (2001). Agricultural influence on landscape sensitivity in the Upper Mississippi River Valley. *Catena*, *42*(2–4), 193–224. https://doi.org/10.1016/s0341-8162(00)00138-7

Lamb, H. H. (1965). The early medieval warm epoch and its sequel. *Palaeogeography, Palaeoclimatology, Palaeoecology*, *1*, 13–37. https://doi.org/10.1016/0031-0182(65)90004-0

Lamb, H. H. (1977). *Climatic history and the future* (Vol. 2). Methuen and Co. Ltd.

Lehner, F., Wood, A. W., Vano, J. A., Lawrence, D. M., Clark, M. P., & Mankin, J. S. (2019). The potential to reduce uncertainty in regional runoff projections from climate models. *Nature Climate Change*, *9*(12), 926–933. https://doi.org/10.1038/s41558-019-0639-x

Leonardi, N., Carnacina, I., Donatelli, C., Ganju, N. K., Plater, A. J., Schuerch, M., & Temmerman, S. (2018). Dynamic interactions between coastal storms and salt marshes: A review. *Geomorphology*, *301*, 92–107. https://doi.org/10.1016/j.geomorph.2017.11.001

Levermann, A. (2014). Climate economics: Make supply chains climate-smart. *Nature*, *506*(7486), 27–29. https://doi.org/10.1038/506027a

Lewis, J. W., Lytle, S. E., & Tavakoly, A. A. (2023). Climate change projections of continental-scale streamflow across the Mississippi River Basin. *Theoretical and Applied Climatology*, *151*(3–4), 1013–1034. https://doi.org/10.1007/s00704-022-04243-w

Lewis, J. W., Tavakoly, A. A., Martin, C. A., & Moore, C. D. (2019). *Mississippi River and tributaries future flood conditions* (Tech. Rep.). ERDC.

Luo, X., Dee, S., Lavenhouse, T., Muñoz, S., & Steiger, N. (2023). Tropical pacific and north Atlantic Sea surface temperature patterns modulate Mississippi Basin hydroclimate extremes over the last millennium. *Geophysical Research Letters*, *50*(2), e2022GL100715. https://doi.org/10.1029/2022gl100715

Luo, X., Dee, S., Stevenson, S., Okumura, Y., Steiger, N., & Parsons, L. (2022). Last millennium ENSO diversity and north American teleconnections: New insights from paleoclimate data assimilation. *Paleoceanography and Paleoclimatology*, *37*(3), e2021PA004283. https://doi.org/10.1029/2021pa004283

Mann, M. E., Zhang, Z., Rutherford, S., Bradley, R. S., Hughes, M. K., Shindell, D., et al. (2009). Global signatures and dynamical origins of the Little Ice Age and Medieval Climate Anomaly. *Science*, *326*(5957), 1256–1260. https://doi.org/10.1126/science.1177303

Martin, J. T., Pederson, G. T., Woodhouse, C. A., Cook, E. R., McCabe, G. J., Anchukaitis, K. J., et al. (2020). Increased drought severity tracks warming in the United States' largest river basin. *Proceedings of the National Academy of Sciences of the United States of America*, *117*(21), 11328–11336. https://doi.org/10.1073/pnas.1916208117

Martin, J. T., Pederson, G. T., Woodhouse, C. A., Cook, E. R., McCabe, G. J., Wise, E. K., et al. (2019). 1200 years of Upper Missouri River streamflow reconstructed from tree rings. *Quaternary Science Reviews*, *224*, 105971. https://doi.org/10.1016/j.quascirev.2019.105971

Marvel, K., Cook, B. I., Bonfils, C., Smerdon, J. E., Williams, A. P., & Liu, H. (2021). Projected changes to hydroclimate seasonality in the continental United States. *Earth's Future*, *9*(9), e2021EF002019. https://doi.org/10.1029/2021ef002019

Milly, P., & Dunne, K. (2001). Trends in evaporation and surface cooling in the Mississippi River Basin. *Geophysical Research Letters*, *28*(7), 1219–1222. https://doi.org/10.1029/2000gl012321

Mishra, V., Cherkauer, K. A., Niyogi, D., Lei, M., Pijanowski, B. C., Ray, D. K., et al. (2010). A regional scale assessment of land use/land cover and climatic changes on water and energy cycle in the upper midwest United States. *International Journal of Climatology*, *30*(13), 2025–2044. https://doi.org/10.1002/joc.2095

Muñoz, S. E., & Dee, S. G. (2017). El Niño increases the risk of lower Mississippi River flooding. *Scientific Reports*, *7*(1), 1–7. https://doi.org/10.1038/s41598-017-01919-6

Muñoz, S. E., Dee, S. G., Luo, X., Haider, M. R., O'Donnell, M., Parazin, B., & Remo, J. W. (2023). Mississippi River low-flows: Context, causes, and future projections. *Environmental Research: Climate*, *2*(3), 031001. https://doi.org/10.1088/2752-5295/acd8e3

Muñoz, S. E., Giosan, L., Therrell, M. D., Remo, J. W., Shen, Z., Sullivan, R. M., et al. (2018). Climatic control of Mississippi River flood hazard amplified by river engineering. *Nature*, *556*(7699), 95–98. https://doi.org/10.1038/nature26145

O'Donnell, M., Doss-Gollin, J., Dee, S., & Muñoz, S. E. (2022). Validation of community earth system model hydrologic variables over the Mississippi River system to understand long term hydrometerologic changes. *AGU Fall Meeting Abstracts*, *2022*, H42E–H1351.

Oleson, K. W. (2010). Technical description of version 4.0 of the community land model (CLM). NCAR Technical Note, 257.

Oleson, K. W., Lawrence, D. M., Bonan, G. B., Drewniak, B., Huang, M., Koven, C. D., et al. (2013). Technical description of version 4.5 of the Community Land Model (CLM), NCAR technical note NCAR/TN-503+STR (Tech. Rep.). https://doi.org/10.5065/D6RR1W7M

Otto-Bliesner, B. L., Brady, E. C., Fasullo, J., Jahn, A., Landrum, L., Stevenson, S., et al. (2016). Climate variability and change since 850 CE: An ensemble approach with the Community Earth System Model. *Bulletin of the American Meteorological Society*, *97*(5), 735–754. https://doi.org/10.1175/bams-d-14-00233.1

Peña-Arancibia, J. L., Bruijnzeel, L. A., Mulligan, M., & Van Dijk, A. I. (2019). Forests as 'sponges' and 'pumps': Assessing the impact of deforestation on dry-season flows across the tropics. *Journal of Hydrology*, *574*, 946–963. https://doi.org/10.1016/j.jhydrol.2019.04.064

Pinter, N., & Heine, R. A. (2005). Hydrodynamic and morphodynamic response to river engineering documented by fixed-discharge analysis, Lower Missouri River, USA. *Journal of Hydrology*, *302*(1–4), 70–91. https://doi.org/10.1016/j.jhydrol.2004.06.039

Pinter, N., Jemberie, A. A., Remo, J. W., Heine, R. A., & Ickes, B. S. (2008). Flood trends and river engineering on the Mississippi River system. *Geophysical Research Letters*, *35*(23). https://doi.org/10.1029/2008gl035987

Pongratz, J., Reick, C., Raddatz, T., & Claussen, M. (2008). A reconstruction of global agricultural areas and land cover for the last millennium. *Global Biogeochemical Cycles*, *22*(3). https://doi.org/10.1029/2007gb003153

Qian, T., Dai, A., & Trenberth, K. E. (2007). Hydroclimatic trends in the Mississippi River Basin from 1948 to 2004. *Journal of Climate*, *20*(18), 4599–4614. https://doi.org/10.1175/jcli4262.1

Quinn, F. H., & Sellinger, C. E. (1990). Lake Michigan record levels of 1838, a present perspective. *Journal of Great Lakes Research*, *16*(1), 133–138. https://doi.org/10.1016/s0380-1330(90)71405-0

Raymond, C., Horton, R. M., Zscheischler, J., Martius, O., AghaKouchak, A., Balch, J., et al. (2020). Understanding and managing connected extreme events. *Nature Climate Change*, *10*(7), 611–621. https://doi.org/10.1038/s41558-020-0790-4

Raymond, P. A., Oh, N.-H., Turner, R. E., & Broussard, W. (2008). Anthropogenically enhanced fluxes of water and carbon from the Mississippi River. *Nature*, *451*(7177), 449–452. https://doi.org/10.1038/nature06505

Rossi, A., Massei, N., Laignel, B., Sebag, D., & Copard, Y. (2009). The response of the Mississippi River to climate fluctuations and reservoir construction as indicated by wavelet analysis of streamflow and suspended-sediment load, 1950–1975. *Journal of Hydrology*, *377*(3–4), 237–244. https://doi.org/10.1016/j.jhydrol.2009.08.032

Rustic, G. T., Koutavas, A., Marchitto, T. M., & Linsley, B. K. (2015). Dynamical excitation of the tropical Pacific Ocean and ENSO variability by Little Ice Age cooling. *Science*, *350*(6267), 1537–1541. https://doi.org/10.1126/science.aac9937

Schilling, K. E., Chan, K.-S., Liu, H., & Zhang, Y.-K. (2010). Quantifying the effect of land use land cover change on increasing discharge in the Upper Mississippi River. *Journal of Hydrology*, *387*(3–4), 343–345. https://doi.org/10.1016/j.jhydrol.2010.04.019

Schilling, K. E., Jha, M. K., Zhang, Y.-K., Gassman, P. W., & Wolter, C. F. (2008). Impact of land use and land cover change on the water balance of a large agricultural watershed: Historical effects and future directions. *Water Resources Research*, *44*(7). https://doi.org/10.1029/2007wr006644

Schneider, U., Finger, P., Meyer-Christoffer, A., Rustemeier, E., Ziese, M., & Becker, A. (2017). Evaluating the hydrological cycle over land using the newly-corrected precipitation climatology from the Global Precipitation Climatology Centre (GPCC). *Atmosphere*, *8*(3), 52. https://doi.org/10.3390/atmos8030052

Schurer, A. P., Hegerl, G. C., Mann, M. E., Tett, S. F., & Phipps, S. J. (2013). Separating forced from chaotic climate variability over the past millennium. *Journal of Climate*, *26*(18), 6954–6973. https://doi.org/10.1175/jcli-d-12-00826.1

Seneviratne, S., Zhang, X., Adnan, M., Badi, W., Dereczynski, C., Di Luca, A., et al. (2021). Weather and climate extreme events in a changing climate [Book Section]. In V. Masson-Delmotte et al. (Eds.), *Climate change 2021: The physical science basis. Contribution of working group i to the sixth assessment report of the intergovernmental panel on climate change* (pp. 1513–1766). Cambridge University Press. https://doi.org/10.1017/9781009157896.013

Smith, A. B. (2020). *U.S. billion-dollar weather and climate disasters, 1980 - present (NCEI accession 0209268)*. NOAA National Centers for Environmental Information. https://doi.org/10.25921/STKW-7W73

Stahle, D. W., Cook, E. R., Burnette, D. J., Torbenson, M. C., Howard, I. M., Griffin, D., et al. (2020). Dynamics, variability, and change in seasonal precipitation reconstructions for north America. *Journal of Climate*, *33*(8), 3173–3195. https://doi.org/10.1175/jcli-d-19-0270.1

Steiger, N. J., Smerdon, J. E., Cook, E. R., & Cook, B. I. (2018). A reconstruction of global hydroclimate and dynamical variables over the Common Era. *Scientific Data*, *5*(1), 1–15. https://doi.org/10.1038/sdata.2018.86

Stevenson, S., Fasullo, J. T., Otto-Bliesner, B. L., Tomas, R. A., & Gao, C. (2017). Role of eruption season in reconciling model and proxy responses to tropical volcanism. *Proceedings of the National Academy of Sciences of the United States of America*, *114*(8), 1822–1826. https://doi.org/10.1073/pnas.1612505114

Stevenson, S., Otto-Bliesner, B., Fasullo, J., & Brady, E. (2016). "El Niño like" hydroclimate responses to last millennium volcanic eruptions. *Journal of Climate*, *29*(8), 2907–2921. https://doi.org/10.1175/JCLI-D-15-0239.1

Stevenson, S., Overpeck, J. T., Fasullo, J., Coats, S., Parsons, L., Otto-Bliesner, B., et al. (2018). Climate variability, volcanic forcing, and last millennium hydroclimate extremes. *Journal of Climate*, *31*(11), 4309–4327. https://doi.org/10.1175/jcli-d-17-0407.1

St. George, S. (2018). *Mississippi rising*. Nature Publishing Group UK.

Swain, D. L., Singh, D., Touma, D., & Diffenbaugh, N. S. (2020). Attributing extreme events to climate change: A new Frontier in a warming world. *One Earth*, *2*(6), 522–527. https://doi.org/10.1016/j.oneear.2020.05.011

Tao, B., Tian, H., Ren, W., Yang, J., Yang, Q., He, R., et al. (2014). Increasing Mississippi River discharge throughout the 21st century influenced by changes in climate, land use, and atmospheric CO2. *Geophysical Research Letters*, *41*(14), 4978–4986. https://doi.org/10.1002/2014gl060361

Tejedor, E., Steiger, N., Smerdon, J. E., Serrano-Notivoli, R., & Vuille, M. (2021a). Global temperature responses to large tropical volcanic eruptions in paleo data assimilation products and climate model simulations over the last millennium. *Paleoceanography and Paleoclimatology*, *36*(4), e2020PA004128. https://doi.org/10.1029/2020pa004128

Tejedor, E., Steiger, N. J., Smerdon, J. E., Serrano-Notivoli, R., & Vuille, M. (2021b). Global hydroclimatic response to tropical volcanic eruptions over the last millennium. *Proceedings of the National Academy of Sciences of the United States of America*, *118*(12), e2019145118. https://doi.org/10.1073/pnas.2019145118

Thiery, W., Davin, E. L., Lawrence, D. M., Hirsch, A. L., Hauser, M., & Seneviratne, S. I. (2017). Present-day irrigation mitigates heat extremes. *Journal of Geophysical Research: Atmospheres*, *122*(3), 1403–1422. https://doi.org/10.1002/2016jd025740

Törnqvist, T. E., Jankowski, K. L., Li, Y.-X., & González, J. L. (2020). Tipping points of Mississippi Delta marshes due to accelerated sea-level rise. *Science Advances*, *6*(21), eaaz5512. https://doi.org/10.1126/sciadv.aaz5512

Touma, D., Stevenson, S., Lehner, F., & Coats, S. (2021). Human-driven greenhouse gas and aerosol emissions cause distinct regional impacts on extreme fire weather. *Nature Communications*, *12*(1), 212. https://doi.org/10.1038/s41467-020-20570-w

Toure, A. M., Luojus, K., Rodell, M., Beaudoing, H., & Getirana, A. (2018). Evaluation of simulated snow and snowmelt timing in the community land model using satellite-based products and streamflow observations. *Journal of Advances in Modeling Earth Systems*, *10*(11), 2933–2951. https://doi.org/10.1029/2018ms001389

Tran, L. T., & O'Neill, R. V. (2013). Detecting the effects of land use/land cover on mean annual streamflow in the Upper Mississippi River Basin, USA. *Journal of Hydrology*, *499*, 82–90. https://doi.org/10.1016/j.jhydrol.2013.06.041

Trouet, V., Esper, J., Graham, N. E., Baker, A., Scourse, J. D., & Frank, D. C. (2009). Persistent positive north Atlantic oscillation mode dominated the medieval climate anomaly. *Science*, *324*(5923), 78–80. https://doi.org/10.1126/science.1166349

Twine, T. E., Kucharik, C. J., & Foley, J. A. (2004). Effects of land cover change on the energy and water balance of the Mississippi River Basin. *Journal of Hydrometeorology*, *5*(4), 640–655. https://doi.org/10.1175/1525-7541(2004)005<0640:eolcco>2.0.co;2

Van der Wiel, K., Kapnick, S. B., Vecchi, G. A., Smith, J. A., Milly, P. C., & Jia, L. (2018). 100-year lower Mississippi floods in a global climate model: Characteristics and future changes. *Journal of Hydrometeorology*, *19*(10), 1547–1563. https://doi.org/10.1175/jhm-d-18-0018.1

Waskom, M., Botvinnik, O., O'Kane, D., Hobson, P., Lukauskas, S., Gemperline, D. C., et al. (2017). Mwaskom/seaborn: V0. 8.1 (September 2017). *Zenodo*.

Werth, D., & Avissar, R. (2002). The local and global effects of amazon deforestation. *Journal of Geophysical Research*, *107*(D20), LBA–55. https://doi.org/10.1029/2001jd000717

Wiman, C., Hamilton, B., Dee, S. G., & Muñoz, S. E. (2021). Reduced Lower Mississippi River discharge during the medieval era. *Geophysical Research Letters*, *48*(3), e2020GL091182. https://doi.org/10.1029/2020gl091182

Zeng, Y., Xie, Z., & Zou, J. (2017). Hydrologic and climatic responses to global anthropogenic groundwater extraction. *Journal of Climate*, *30*(1), 71–90. https://doi.org/10.1175/jcli-d-16-0209.1

Zhang, Y.-K., & Schilling, K. (2006). Increasing streamflow and baseflow in Mississippi River since the 1940s: Effect of land use change. *Journal of Hydrology*, *324*(1–4), 412–422. https://doi.org/10.1016/j.jhydrol.2005.09.033